AD-A053 208 UTAH STATE UNIV LOGAN DEPT OF CHEMISTRY AND BIOCHEMISTRY F/G 20/4
DESIGN AND FABRICATION OF A PROTOTYPE COLD BACKGROUND EXPERIMEN--ETC(U)
DEC 77 W M MOORE F19628-72-C-0317

UNCLASSIFIED AFGL-TR-77-0306 NL

1 OF 1
AD A053208

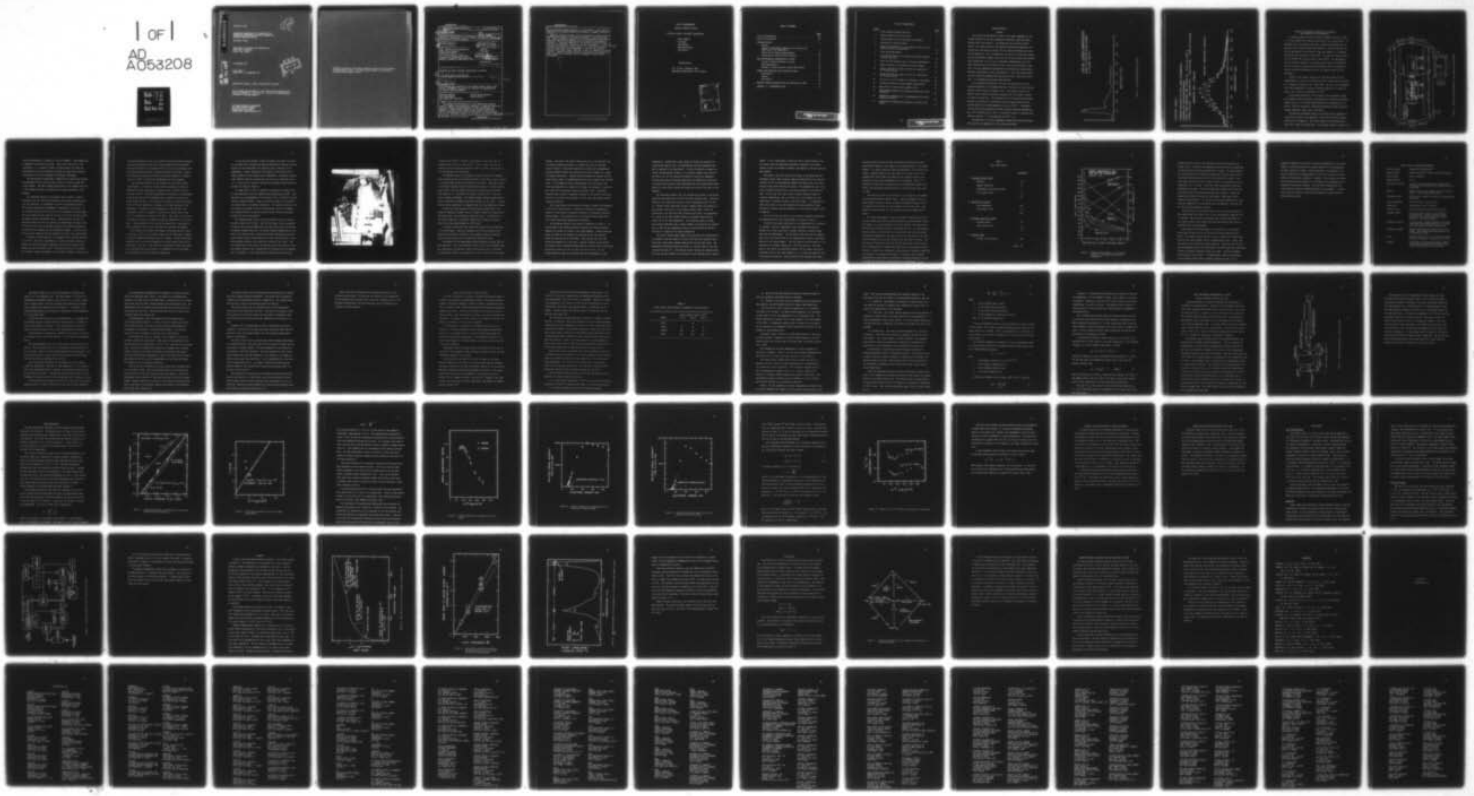

END
DATE FILMED
6-78
DDC

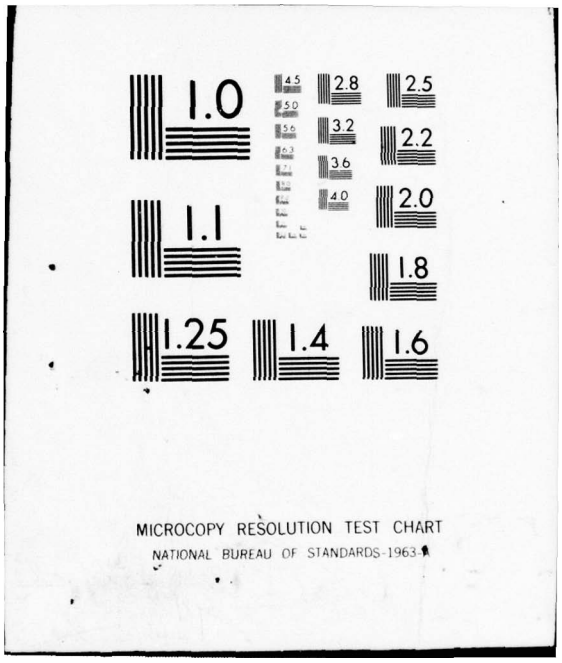
1.0
1.1
1.25
1.4
1.6
1.8
2.0
2.2
2.5
2.8
3.2
3.6
4.0
4.5
5.0
5.6
6.3
7.1
8.0
9.0
MICROCOPY RESOLUTION TEST CHART
NATIONAL BUREAU OF STANDARDS-1963-A

AFGL-TR-77-0306

DESIGN AND FABRICATION OF A PROTOTYPE COLD BACKGROUND EXPERIMENTAL REACTION CHAMBER AND SPECTRAL DETECTION SYSTEM

William M. Moore

Department of Chemistry and Biochemistry
Utah State University
Logan, Utah 84322

31 December 1977

Final Report
4 May 1972 - 30 September 1977

This research was sponsored by the Defense Nuclear Agency under Subtask I25BAXHX632, Work Unit 08, entitled "IR Phenomenology and Optical Code Development."

AIR FORCE GEOPHYSICS LABORATORY
AIR FORCE SYSTEMS COMMAND
UNITED STATES AIR FORCE
HANSCOM AFB, MASSACHUSETTS 01731

UNCLASSIFIED

SECURITY CLASSIFICATION OF THIS PAGE (When Data Entered)

REPORT DOCUMENTATION PAGE	READ INSTRUCTIONS BEFORE COMPLETING FORM
1. REPORT NUMBER: AFGL-TR-77-0306	2. GOVT ACCESSION NO. / 3. RECIPIENT'S CATALOG NUMBER
4. TITLE (and Subtitle): Design and Fabrication of a Prototype Cold Background Experimental Reaction Chamber and Spectral Detection System	5. TYPE OF REPORT & PERIOD COVERED: Final Report, 4 May 72 - 30 Sep 77 / 6. PERFORMING ORG. REPORT NUMBER
7. AUTHOR(s): William M. Moore	8. CONTRACT OR GRANT NUMBER(s): F19628-72-C-0317
9. PERFORMING ORGANIZATION NAME AND ADDRESS: Dept. Chemistry and Biochemistry, Utah State University, Logan, Utah 84322	10. PROGRAM ELEMENT, PROJECT, TASK AREA & WORK UNIT NUMBERS: 62704 H, CDNA 09AA
11. CONTROLLING OFFICE NAME AND ADDRESS: Air Force Geophysics Laboratory, Hanscom AFB, Massachusetts 01731, Monitor / Francis P. Del Greco / OPR	12. REPORT DATE: 31 Dec 77 / 13. NUMBER OF PAGES: 83 (268 p.)
14. MONITORING AGENCY NAME & ADDRESS (if different from Controlling Office)	15. SECURITY CLASS (of this report): Unclassified / 15a. DECLASSIFICATION DOWNGRADING SCHEDULE

16. DISTRIBUTION STATEMENT (of this Report)

Approved for public release; distribution unlimited

CDNA, I25BAXH

17. DISTRIBUTION STATEMENT (of the abstract entered in Block 20, if different from Report)

09, X632

18. SUPPLEMENTARY NOTES

This research was sponsored by the Defense Nuclear Agency under Subtask I25BAXHX632, Work Unit 08, entitled "IR Phenomenology and Optical Code Development."

19. KEY WORDS (Continue on reverse side if necessary and identify by block number)

Chemiluminescence
Mass spectrometry
Low temperature reactions
Atomic oxygen detection
Ozone detection

20. ABSTRACT (Continue on reverse side if necessary and identify by block number)

The design and fabrication of a low temperature chemical reaction chamber was successfully completed. A spectral detection system to observe chemiluminescence in the infrared was also completed. Sample spectra taken in the finished chamber are shown to demonstrate the potential application of the apparatus. The optical components present at the time of the project completion

→ over

DD FORM 1 JAN 73 1473 EDITION OF 1 NOV 65 IS OBSOLETE

UNCLASSIFIED

SECURITY CLASSIFICATION OF THIS PAGE (When Data Entered)

362 175

date permitted spectral detection to 12 micrometers. The limiting sensitivity for excited species is estimated at a number density of $10^7 cc^{-1}$.

Several detection schemes have been examined to measure atomic and molecular species in the reaction chamber or from the exhaust gas. Mass spectrometry appears to be very promising in cases where molecular beams can be modulated and ion counting techniques are employed. A nonlinear response for the molecular species O_3^+ has limited the usefulness of positive ion mass spectrometry. A new technique for measuring atomic oxygen *in situ* has been developed, but the sensitivity is not comparable to that for the infrared emission from atomic oxygen reactions in the low temperature Cochise facility. Negative surface ionization has potential advantages for some of species of interest and this technique is under further development.

LIST OF CONTRIBUTORS

Contract F19628-72-C-0317

William M. Moore, Principal Investigator

Peter Codella
Don Goode
Lee Handley
Kathleen Knierim
Clair Wyatt

Subcontractors

A.D. Little, Cambridge, Mass.
Minuteman Laboratories, Act on, Mass.

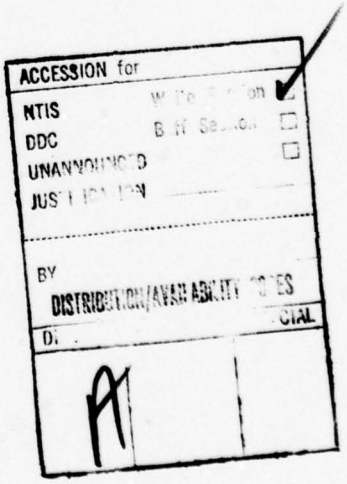

TABLE OF CONTENTS

LIST OF ILLUSTRATIONS

COCHISE FACILITY

General

The design and fabrication of many of the major components in the Cochise facility at Air Force Geophysics Laboratory (OPR) were accomplished under this contract. The exceptions were the outer vacuum housing and vacuum system for the complete experimental apparatus, the closed cycle refrigeration system, and the computer hardware and interfacing components. The low temperature shrouds for the reaction chamber and the spectrometer chamber along with the reaction vessel were designed under subcontract to A.D. Little, Cambridge, Massachusetts, and they were constructed by the EDL machine shop, Utah State University, Logan, Utah. The low temperature spectrometer was designed and constructed by Minuteman Laboratories, Acton, Massachusetts. The liquid helium cooled detector system was designed and constructed by EDL, Utah State University. All components met design specifications.

The successful construction, delivery, and operation of all the required components can be demonstrated most vividly by the two infrared emission spectra shown in Figures 1 and 2. The Cochise facility can measure excited state distributions unaffected by collisional, surface, or radiative relaxation. The sensitivity with the liquid helium cooled detector is sufficient to spectrally resolve infrared radiation from excited species with number densities as low as $10^7 cc^{-1}$. Preliminary results from those experiments have been recently reported (Kennealy et al., 1977; DelGreco et al., 1977). As shown in Figure 2, radiation from states as high as v = 13 are observed for $N(^2D) + O_2$.

Descriptions of the major components designed and constructed under this contract are summarized in the following sections.

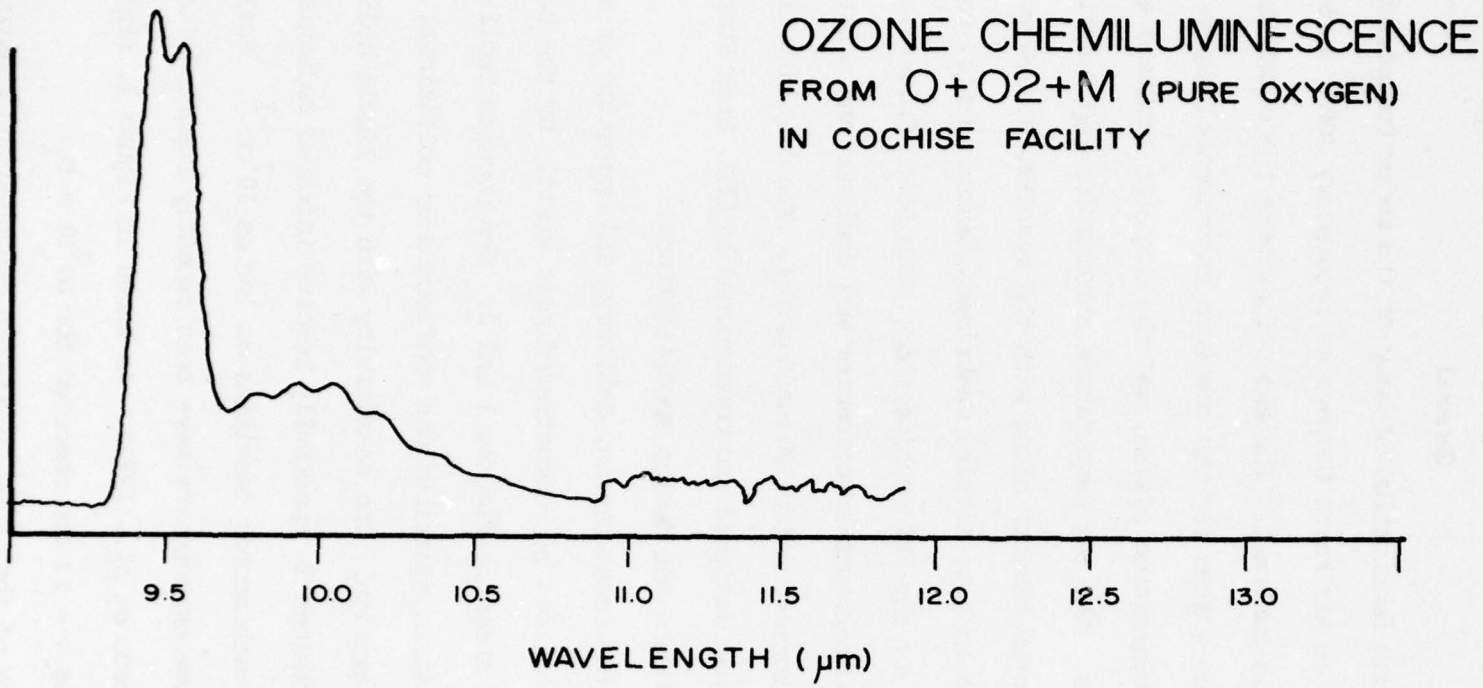

Figure 1. Ozone chemiluminescence spectrum.

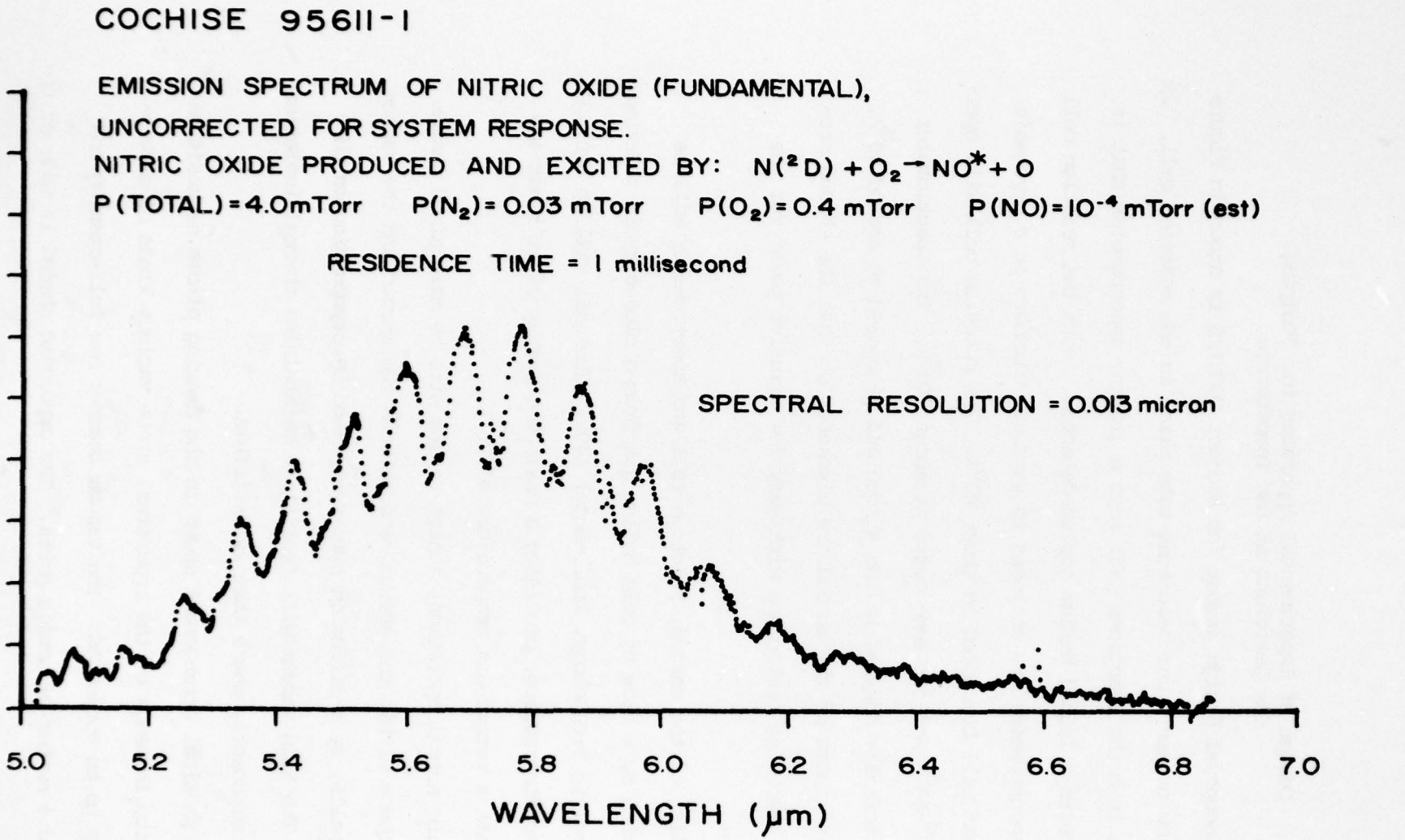

Figure 2. Emission spectrum of nitric oxide.

Design of Experimental Apparatus for Studying Gas Reactions at Low Temperature

A conceptual design layout for Project COCHISE is shown in Figure 3. The low pressure gas reactions take place in the reaction cell. IR emissions from the reactions pass into a grating spectrometer that is equipped with a liquid helium cooled detector. Both the reaction cell and the spectrometer are enclosed in separate chambers in a cryogenic shroud that will be cooled to about $20^{\circ}K$. The reaction cell will operate at 20°-$60^{\circ}K$ and for some tests at about $300^{\circ}K$. The spectrometer will be thermally coupled to the shroud and be cooled to around $20^{\circ}K$. Interior surfaces of the shroud are blackened so that the shroud provides an absorbing background with very low emissive power for the experiment.

Cooling of the shroud, reaction cell and spectrometer will be accomplished by a flow of cold helium gas from a closed cycle refrigerator, Cryogenic Technology, Inc., Model 1400. The unit will be equipped with three compressors, providing a maximum capacity of at least 450 watts, with a return gas temperature of $20^{\circ}K$.

During normal operation, a high vacuum will be maintained inside both chambers within the shroud, and between the shroud and the vacuum chamber walls, by a diffusion pump system and by cryopumping on the shroud. The high vacuum will facilitate maintaining thermal isolation between components, where that is desirable.

The physical arrangement shown in the drawing places emphasis on flexibility in usage of the apparatus, since various kinds of experiments are to be conducted. The vacuum chamber has full-opening end doors and a number of access ports. The cryogenic shroud is made of two

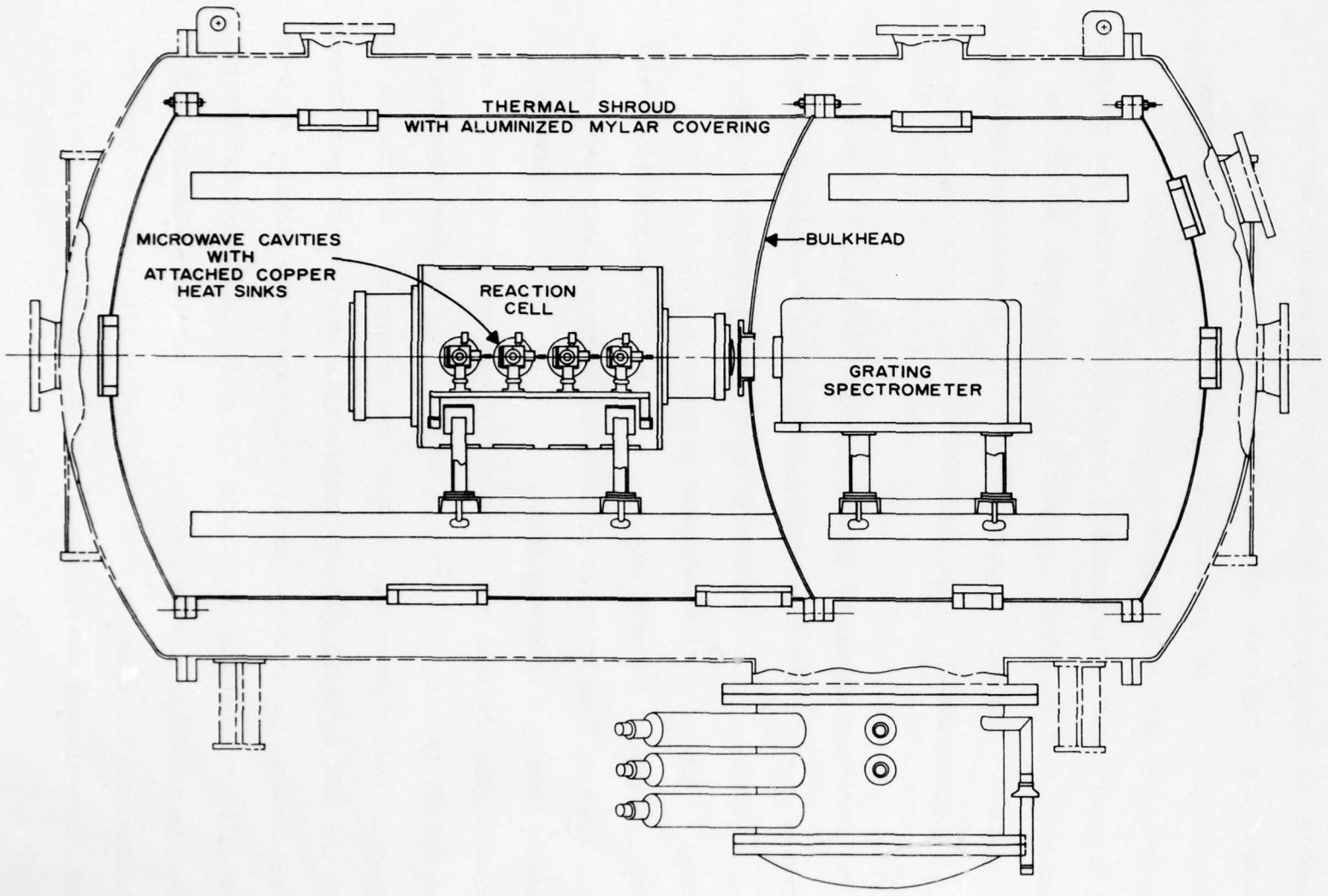

Figure 3. Diagram of vacuum chamber for low temperature experiments.

sections separated by a bulkhead to form two chambers. Each chamber has a removable, full-opening end cover. Most of the services for the experiment, i.e., cryogenic coolant, microwave power, gas flows and instrumentation, will be brought in through the large side and bottom access ports, as will be discussed in subsequent paragraphs.

The spectrometer incorporates a mechanism for rotating the grating. The mechanism will be driven through a shaft, by a motor outside the vacuum chamber. The shaft passes through ports in the chamber wall and in the cryogenic shroud, as indicated by the shaft centerline in the drawing.

The conceptual design of the reaction cell is shown in Figure 3. The ends of the cell and four rectangular ports on the cylindrical portion are removable, to accommodate a variety of experimental setups. One possible experimental arrangement is depicted in the drawing. In it, gas flow enters the cell from four sets of opposing injection tubes. The gas entering from the tubes on one side of the cell has been ionized by passing through a microwave cavity. Emissions resulting from the reactions within the cell are viewed by the spectrometer through a lens at one end of the cell and through a window in the bulkhead separating the reaction cell chamber and the spectrometer chamber. A mirror at the end of the cell opposite the lens enhances the input to the spectrometer.

Ultimately, the injected gas is cryopumped on the interior surfaces of the cell. The cell is provided with a series of annular baffles to improve the molecular capture probability and minimize molecular backscattering into the reaction zone. The baffles also serve to increase the effective thermal absorptance of the interior surface of the cell and

to provide shielding, so that the transfer of spurious thermal radiation from the gas-injection tubes into the spectrometer will be minimized. The lens and mirror at the opposite ends of the cell are mounted to the end plates through thermally isolating stainless steel tubes. Heaters on the mounting flanges will maintain the optical elements at temperatures of 50-100^{o}K to prevent gas condensation on their surfaces.

The cylindrical portion of the reaction cell will have coolant tubes bonded to its exterior surface as well as heaters, so that its temperature can be controlled to a desired value to within $\pm 0.1^{o}$K in the range 20-60^{o}K. The higher temperatures are required for experiments in which gas injection is terminated after a quantity of gas is condensed inside the cell. The pressure in the cell can then be controlled by the cell-wall temperature, according to the vapor pressure of the condensate. To control the cell temperature to the set point, the refrigerator circuit is adjusted so that with no heater input to the cell, its temperature is below the set point. Heat input via the electric heaters is used as a trimmer to bring the temperature up to the set point. The temperature of the cell can be sensed with a thermistor(s), which provides an input to the controller that operates the heaters.

The cylinder, the baffles, the flanges, end plates and port covers of the cell, as well as the coolant tubes, will be fabricated of copper, to minimize temperature gradients over the surface. Design calculations indicate that it will not be necessary to provide coolant tubes on the end plates of the cell. With indium foil compressed between the flanges on the cylinder and the end plates, the temperature of the end plates will be within 0.1^{o}K of the cylinder temperature.

It has not been possible, within the scope of our work, to arrive at a cylinder wall thickness and cooling tube pattern that would clearly achieve the near-isothermal wall condition that is desired for the experiments. Further analysis of this aspect of the design will be required before a final design can be established. Preliminary calculations indicate that the cylinder wall may have to be relatively thick, i.e., ½ inch or more. Parallel circuits and peripheral wraps around the cylinder are shown in Figure 4.

For some tests, it will be desirable to operate the reaction cell at room temperature with the cryogenic shroud maintained at 20°K. Such operation can be accommodated if the reaction cell is thermally isolated from the cryogenic shroud. Hence, the mounting frame for the reaction cell should have a low thermal conductance. The exterior surface of the cell should be polished to have a low emittance, and also be wrapped with aluminized Mylar to provide further thermal radiation shielding between the cell and the shroud.

The estimated power input into each microwave cavity for the gas injection tubes is 20-30 watts. Most of this input will be dissipated as heat in the gas and transferred to the tube walls within the cavity. Preliminary analyses show that, to prevent elevated temperatures in the cavity, the tube must have a much better thermal conductivity than the glass normally used in setups operating at room temperature and 1 atmosphere ambient pressure, with forced air cooling of the cavity. Low tube temperatures in the cavity are desired so that the amount of spurious thermal radiation that is piped down the tube and into the reaction cell is minimized. On the other hand, we estimate that for the gas

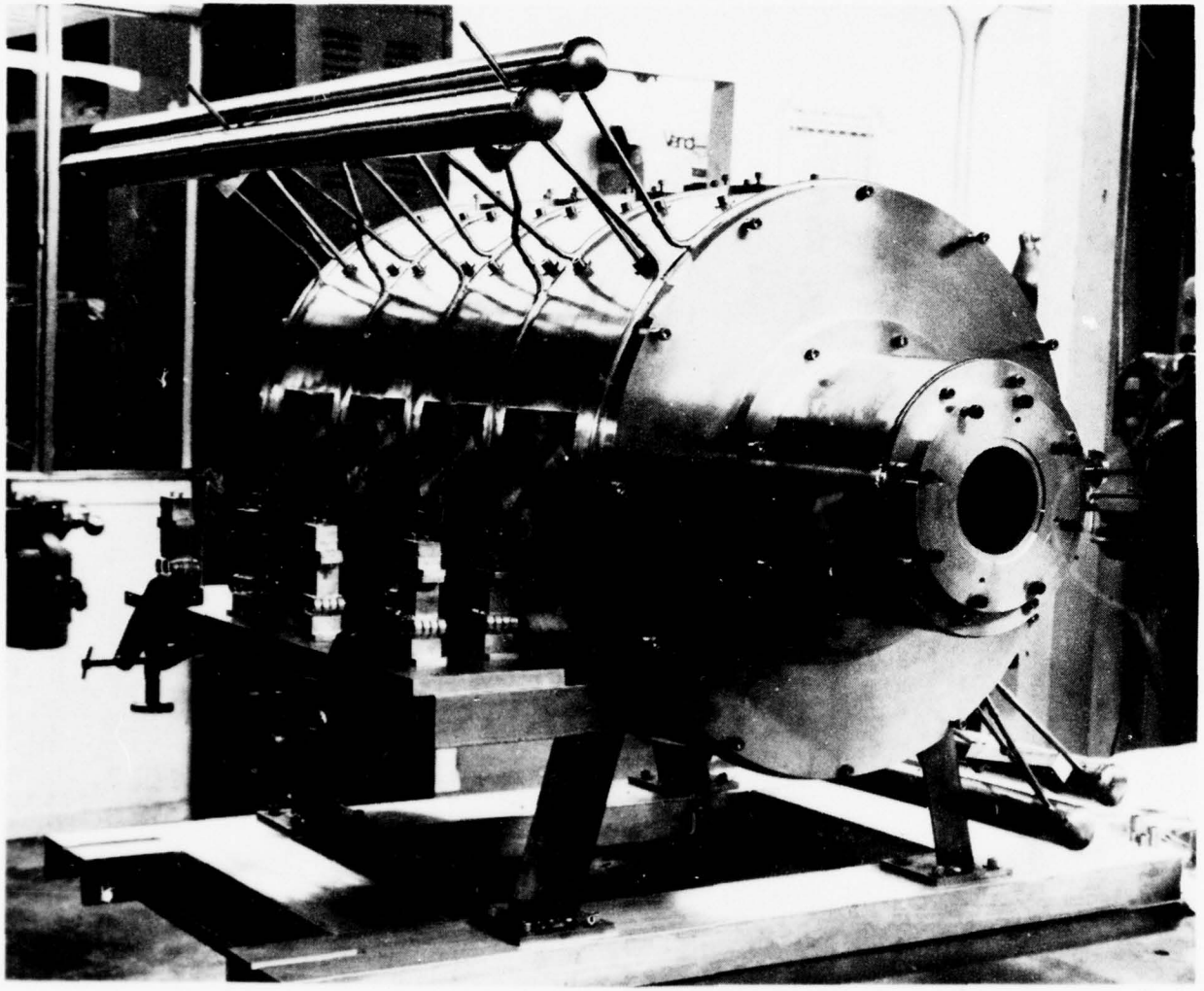

Figure 4. Photograph of reaction vessel showing tubing for cooling gases (upper left), ports for microwave cavities (middle left), and observation opening (middle right).

injection flow rates of interest, the pressure in the tubes near the injection point will be in the order of 1 torr. Hence, the tube temperature must be maintained above about $60^{\circ}K$ to prevent condensation of the injected gas on the tube wall.

The approach shown in the drawing is based on the use of sapphire tubes passing through the microwave cavities. Each tube is heat-stationed to a cooled copper block on both sides of the cavity. The copper blocks are thermally coupled through flexible copper straps to a fairly massive copper plate, that is cooled by the flow of cold helium gas through a tube bonded to it. The plate will operate at about $25^{\circ}K$ or less and will be roughly isothermal. The flexible copper thermal straps would be sized to maintain the copper block heat stations at about $60^{\circ}K$. Electric heaters can be attached to the copper blocks for fine temperature control.

To keep the lines carrying the input gas above about $60^{\circ}K$, they should be thermally isolated from the cryogenic shroud, by wrapping with aluminized Mylar, and provided with some heat input. In addition, as the drawing indicates, a thermally isolated port should be utilized where these lines pass through the $20^{\circ}K$ shroud.

It should be noted that the reaction cell need not be vacuum-tight in the usual sense. Small out leakages from the cell would be cryopumped on the interior surfaces of the cryogenic shroud at such high speed that high vacuum would be maintained outside the cell.

The detector in the spectrometer requires cooling to below $10^{\circ}K$ for best operation. Since refrigeration at this level is not available from the closed-cycle refrigerator, liquid helium cooling must be provided. A liquid helium vessel is suspended from a port in the top of the vacuum

chamber. The neck of the vessel, which serves as a fill-and-vent line, is flexibly connected by means of a bellows to a port in the 20°K shroud to effect a light-tight penetration, while still accommodating relative movement between the shroud and the vacuum chamber as a result of thermal contractions. Thermal coupling between the detector and the liquid helium vessel is accomplished by high purity copper wires (99.999% pure). As an example of their effectiveness, four such wires, with 0.060 inch diameter and a length of 30 inches, will conduct 0.1 watts of heat flow with a temperature drop of only about 1.2°K. Particular attention must be paid to mechanical coupling of the wires to the detector and to the liquid helium vessel to insure that high thermal conductances are achieved.

This liquid helium cooling system is simple, reliable and economical in the use of liquid helium. It avoids the necessity of temperature control or flow control as would be required in a continuous flow-type cooling system. Only periodic fill of the liquid helium vessel every two or three days during operation is necessary.

The conceptual design of the shroud is indicated in Figure 3. The two sections of the shroud forming the reaction cell and spectrometer chambers are mounted on tracks in the vacuum chamber. Thermal-isolation blocks, as shown in the drawing, are provided at the four mounting points for each section of the shroud. They maintain the heat leak through the supports at a low level. Exterior surfaces of the shroud are covered with an insulating spacer material (such as used in multilayer insulation systems) and with an aluminized mylar shield, to limit thermal radiative input to the shroud from the surroundings at room

temperature. Longitudinal tracks inside the shroud are provided for mounting the reaction cell, the spectrometer and other equipment that may be required in the experiments. It may be desirable to pressurize either the spectrometer chamber or the reaction chamber with helium to the level 1-10 torr to accelerate cooldown or warm-up of components. The end covers and the bulkhead separating the chambers are configured to withstand the pressure loads associated with such pressurization when there is a high vacuum outside the shroud and in one or the other of the chambers.

Our experience suggests that the cylindrical portions of the shroud should be fabricated from 1/8 inch thick 6061 aluminum alloy. Effective cooling of the cylindrical portions can be accomplished with 1/2 inch I.D. coolant tubing (prefarably D-type) wrapped around the periphery of the cylinder, with about 12 inch spacing between tubes. With this spacing and a 1/8 inch thick 6061 aluminum alloy shell, the temperature at a point on the shell midway between two adjacent tubes would be within $1^{o}K$ of the tube temperature. The resulting length of tubing would provide excellent heat transfer between the shroud and the coolant gas, so that the gas temperature leaving the shroud would be within a fraction of a degree of the shroud temperature.

The use of coolant tubes bonded to the end covers of the shroud can be avoided if they are made of 1/8 inch thick type 1100 aluminum alloy, which has a much higher thermal conductivity than the 6061 alloy. The temperature difference between the center of the end cover and the edge would be less than $1^{o}K$. Good thermal contact between the flanges on the end cover and the flanges on the cylinder can be achieved with an indium

gasket. It is a convenience to avoid the use of cooling tubes on the end covers since the associated disconnect couplings in the helium cooling circuit are thereby eliminated, and removal of the end covers is made simpler.

The seals on the ports and the end covers of the shroud must be reasonably vacuum tight to permit moderate pressurization of either the reaction cell or the spectrometer chamber with helium gas, while maintaining a high vacuum outside the shroud. We recommend that all of the ports, including the end covers, be sealed by means of an indium wire seal. We have used this type of seal on small diameter flanges at cryogenic temperatures, and on a flange of 12 inch diameter at room temperature, to achieve reliable, high vacuum seals. In comparison to other metal seals, it has the advantages that only moderate flange loadings are required and the preparation of the flange surfaces is not as exacting.

All of the covers on ports in the shroud are removable through the corresponding port in the vacuum chamber, as shown in Figure 3.

A means of initially evacuating the two compartments in the shroud is required. During an experiment these evacuation lines must be blocked off in such a way that no thermal radiation is piped through them into the compartments. The evacuation lines from the two compartments run to the outlet ports of two extended stem valves in the bottom housing of the vacuum chamber. The valve bodies are maintained at a low temperature via thermal coupling to a $20^{\circ}K$ heat station. The inlet ports of the valves are manifolded together and the common line can be connected either to the vacuum chamber or to a helium gas supply by valving outside the housing. During evacuation the extended stem valves

and the evacuation valve are open, connecting the reaction cell and spectrometer chambers to the vacuum in the bottom housing of the vacuum chamber. For normal operation during an experiment, all the valves are closed. Thermal radiation from warm lines on the inlet side of the extended stem valves cannot be piped into the cryogenic shroud, and emission from the valves themselves will be negligible. When it is desirable to pressurize the reaction cell or spectrometer chamber with helium, the appropriate extended stem valve and the helium input valve are open.

Cold Helium gas from the refrigerator is circulated to the chamber through vacuum-jacketed transfer lines. Inside the chamber there are three parallel circuits; one for cooling the cryogenic shroud, one for the reaction cell and one for the microwave cavities heat sink. Heat loads for various elements in the cooling circuits are summarized in Table 1.

For certain experiments it may be desirable to operate with the return gas temperature from the various circuits at quite different levels. For example, it may be desirable to have the reaction cell operating at $60^{o}K$ while the cryogenic shroud is maintained at $20^{o}K$. The refrigerator characteristics are such that, for a given total heat load (and number of operating compressors), the temperature of the gas going to the load, and the temperature of the gas returning from the load, are fixed. The heat loads in the parallel circuits and the flow rates to the circuits must be apportioned in a manner consistent with the refrigerator characteristics. Despite this constraint a wide variety of operating conditions are possible, as illustrated by Figure 5. The Figure shows possible combinations of heat loads for two parallel circuits obtainable with the CTI Model 1400 refrigerator operating with two compressors. It is

TABLE I

Heat Loads Summary

	Load-Watts
1. Cryogenic Shroud Circuit	
Radiation	90
Support conduction	17
Spectrometer grating drive shaft	3
Flow control valve	3
	113
2. Reaction Cell Circuit	
Gas condensation	106
Flow control valve	3
	109
3. Microwave Heat Sink Circuit	
Microwave power	90
Flow control valve	3
	93
4. Transfer Lines	
50 feet at 0.5 watts/ft	25
TOTAL	340

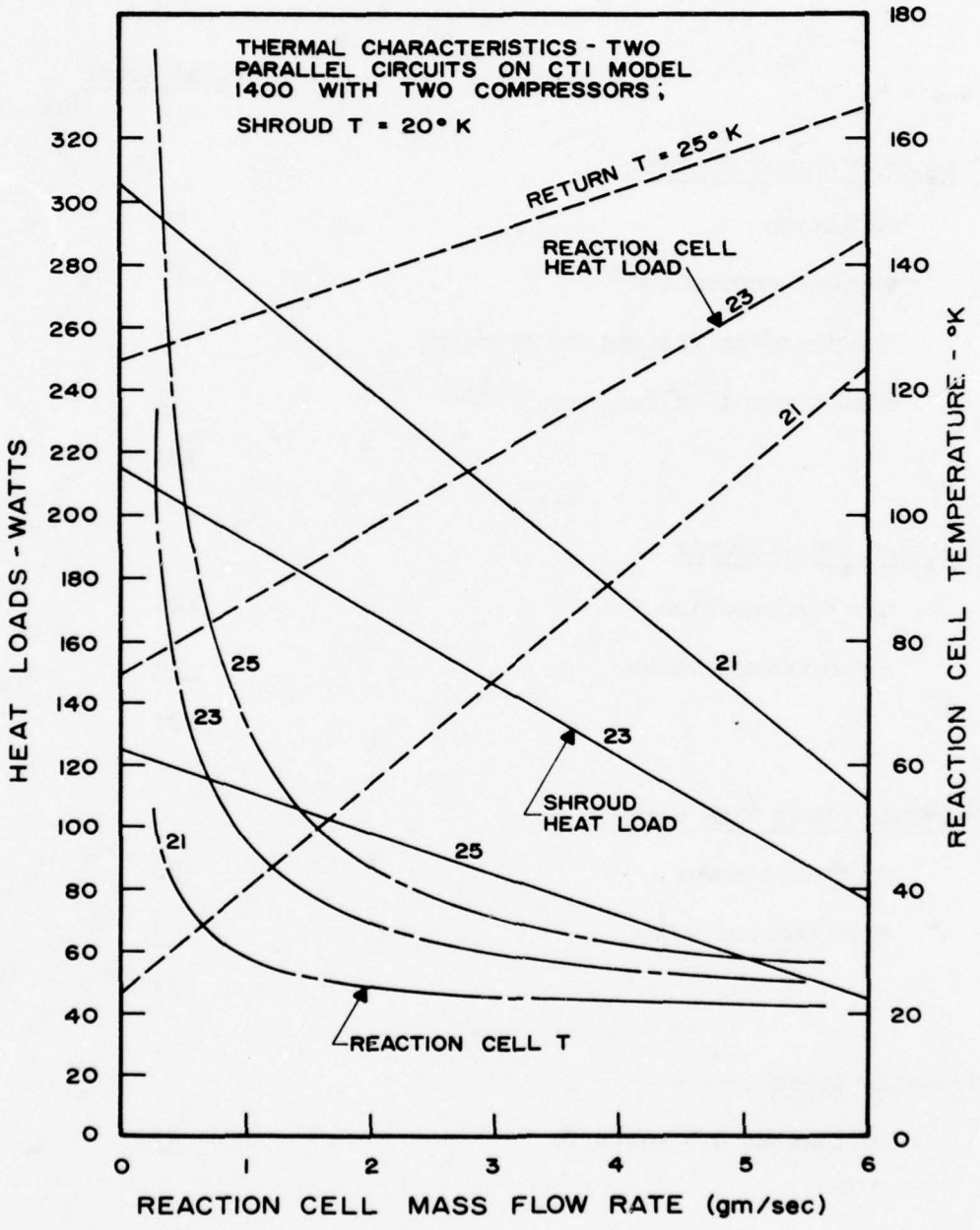

Figure 5. Thermal Characteristics - two parallel circuits on CTI Model 1400 with two compressors.

assumed that one circuit is the cryogenic shroud, and the other the reaction cell. The return gas temperature from the shroud is maintained at 20°K while that from the reaction cell is varied. The heat loads on the two circuits and the return gas temperature from the reaction cell are plotted versus mass flow rate to the reaction cell circuit. The total mass flow rate for both circuits is fixed, for operation with two compressors, at 9.3 gm/sec. Curves for three refrigerator return gas temperatures are shown. The latter temperature results from mixing the gas flows through the shroud and reaction cell circuits. Return gas temperatures outside the range of, and between, those shown in the Figure are also possible. It can be seen that many combinations of heat loads and temperature of the reaction cell are possible. The same will be true with three parallel circuits.

According to CTI, the pressure drop of the gas flowing through the heat loads should not exceed 2 psi, if full refrigeration capacity is to be achieved. The tube sizes and lengths that have been described for the crogenic shroud, the reaction cell and the microwave heat sink are consistent with this requirement.

Heat inputs to the spectrometer will come from the two stepping motors used to adjust the slits and from the grating mechanism drive shaft. The stepping motors operate for only a fraction of a second when the slits are being changed, and at a moderate power level. Hence, this heat input can be ignored for normal operation. The drive shaft for the grating mechanism will be heat stationed to the 20°K shroud and constructed to have low thermal conductance along its length. The heat inleakage from this shaft will be small. The spectrometer frame will be mounted on the cryogenic shroud with a thermally conducting mount, so its

temperature should be very close to the shroud temperature at all times. However, cool-down and warm-up of optical elements in the spectrometer has been a matter of concern. During cool-down of the apparatus, the optical elements can be accomplished in a few hours, and this is acceptable from an operating standpoint. However, if the elements are colder than the housing during warm-up, it is possible that contaminants will condense on the optical surfaces. To avoid such contamination, provision should be made for attaching heaters to each element. If necessary these can be used to insure that the element is warmer than the housing during warm-up.

Twenty Kelvin, Scanning Monochromator

Optical system:	Asymmetrical Czerny-Turner
Optical design:	Coma-corrected with re-entry spectra eliminated.
Focal length:	500 mm. (nominal)
Aperture ratio:	f/6.9
Diffraction grating:	75 g/mm., 12 micron blaze, 64 x 64 mm. ruled area, original grating ruled in aluminum and gold overcoated.
Mirrors:	Quartz, 500 mm. focal length, concave, with gold coating. Mirror back coated with al.
Wavelength range:	With 75 g/mm. grating, zero-order to approximately 20 microns.
Linear dispersion:	267 A/mm. with 75 g/mm. grating.
Resolution:	Approximately 25A @ 10 microns.
Scanning drive:	Sine drive type with precision lead screw.
Scanning speeds:	Six- 0.01, 0.025, 0.05, 0.1, 0.25 and 0.5 microns/minute. Scanning speeds selected externally with gear box and motor located external to the vacuum system.
Wavelength readout:	5 digit counter located externally with least significant digit equivalent to 10A. Counter will have higher and lower safety limits.
Wavelength encoder:	Located externally and coupled to the drive system. Will produce pulse equivalent to LSD of wavelength counter.
Slits:	Multiple fixed slits with slit position readout and control external. Six slits 0.1 to 3 mm.
Housing:	Light tight aluminum housing bellows coupled to monochromator, baffled to minimize stray light with provisions for adding vents.

The design concept is to utilize monochromator technology and adapt it for low temperature use. The basic concept is to mount the monochromator components (optics, slits, drive, etc.) in such a manner that a minimum change in optical alignment and wavelength calibration occurs between room temperature and 20 degrees K. In addition, the proposed design permits easy removal or installation of the monochromator in the AFCRL dewar.

The optical design chosen for the monochromator is an asymmetrical Czerny-Turner system, coma-corrected for the wavelength of primary interest (approximately 10 microns). This correction point also corresponds to the blaze angle of the grating (approximately 25 degrees).

Coma-correction is achieved by a change in the radius of curvature and off-axis angle of one of the mirrors. In this case, the collimating mirror.

The grating supplied will be a 75 g/mm. plane grating blazed at 12 microns. The blaze angle will be a 26.75 degrees and the grating will be an original, ruled on a solid aluminum blank and gold overcoated. The ruled area will be 68 x 68 mm. and with this grating the monochromator will have an effective aperture ratio of f/6.9.

With this grating installed, the instrument will have a normal reciprocal dispersion of 268 A/mm. at room temperature. At 20 degrees K. and at the wavelength region of interest, the reciprocal dispersion will be approximately 242 A/mm. Gratings for the cold monochromator will be kinematically mounted and will be interchangeable with a minimum of effort.

The collimating and focusing mirrors will be half-meter focal length, spherical mirrors of quartz (fused silica) and will be gold overcoated.

The monochromator components will be mounted on a frame fabricated from a low expansion metal (Invar). The frame will be kinematically mounted to the base plate in the AFCRL dewar. This mount will be a three point mount with one point located directly below the entrance slit. The second point will be located along the entrance axis and will be free to move along this axis only. The third point will be free to move in any direction except the vertical one.

The monochromator frame and components will be covered with a light tight aluminum housing. In order to make the system light tight, the entrance and exit slits and the scanning drive feed-through will be coupled to the housing by stainless steel bellows. Two accessory ports will also be provided in the rear wall of the housing.

The entrance and exit slit assemblies will consist of a disc containing at least six, fixed slits. These slits will be machined in the disc and will vary in width from 0.1 mm. to 3 mm. Each slit will be 20 mm. high. Slits will be indexed into position by a stepping motor located directly above the slit plate and coupled to the plate by spur gears. Each slit position will correspond to 1 step of the motor and the actual positioning of the slit will be accomplished by a ball and leaf spring. Slit selection will be remotely controlled.

Each mirror will be mounted in an Invar frame that is mounted directly to the basic frame. The mirror mounting will be a three point one and the mirror will be held in place by BeCu leaf springs. Fine mirror adjustments will be provided in the mirror mask and will be Kel-F tipped screws. Thermal coupling of the mirrors will be made by metallizing the back of each mirror and thermally coupling this coating to the monochromator frame with a copper wire.

The grating holder will be fabricated from aluminum and will contain the three classical grating adjustments. The holder will be thermally coupled to the monochromator frame by a copper wire. The grating blank will be held in place in the holder by BeCu leaf springs.

The grating mount will be a permanent part of the monochromator frame and will be fabricated from Invar. The mount will contain a kinematic mount for the grating holders and this mount is designed so that the net motion of the grating from room temperature to 20 degrees K. is zero.

Scanning will be accomplished by using a conventional sine-drive mechanism. The drive will be controlled from outside the dewar and will provide at least six scanning speeds, with the minimum scanning speed being 0.1 microns/min.

The drive screw will be a precision ball screw designed specifically for cryogenic service. The screw and nut will be made of Inconel and the balls made of titanium carbide. The screw assembly will be coated with an inorganic, solid film lubricant. The major reasons for loss of wavelength calibration from room temperature to 20 degrees K. are change in grating spacing and lead screw pitch. If not compensated for, this shift will be approximately 700 A. By properly selecting the materials and mounting method of the scanning drive system this wavelength shift can be held to less than 50 A.

The scanning drive controls will be located outside the vacuum system and will consist of a power switch, scan direction switch, a wavelength counter with the least significant digit equivalent to 10 A., at least six, selectable scanning speeds and an optical pulse generator that will produce an electrical pulse every 20 A.

Stray light will be minimized in the system by baffling at the entrance and exit ports. In addition, the interior of the monochromator and housing will be coated with a flat black, bakeable finish. All bearings, bearing mounts and any moving parts will be coated with an inorganic dry film lubricant.

Liquid Helium Cooled Infrared Detector

The LSP-1 consists of two units, a preamplifier-detector module, a console, and associated interconnecting cables. The module contains a parabolic reflecting condenser, volume IR detector, operational amplifier, IR emitting diode, temperature monitors and associated electronic elements and devices. The console provides system control functions, detector bias, signal conditioning circuitry, and output indicators and terminals. The console is battery operated to simplify the system and reduce the probability of 60-Hz noise problems.

The preamplifier is designed to be mounted onto the exit slit flange of a Minuteman Laboratories Model 305M scanning monochromator, which is to be installed within a cryogenic high-vacuum system and cooled to liquid helium temperatures. The parabolic reflector is an f/0.25 which images the f/8 monochromator 2-cm high exit slit onto the 3.0-mm cubic detector.

Appropriate cabling, passing through the radiation shield and vacuum wall of the cryogenic system, provides for remote control and data acquisition adjacent to the system.

The preamplifier utilized in the LSP-1 is known as the transimpedance amplifier (TIA) which is a direct-coupled negative-feedback operational scheme that has been successfully applied to the ultra-high impedance cryogenically-cooled photoconductive detectors. The general requirements placed upon the preamplifier input device are that it exhibit very low leakage currents (less than 10^{-12} amperes), have good ac gain, very low noise, low input capacitance, and operate at temperatures as low as $4.2^{\circ}K$.

Several devices satisfy these requirements to some degree. The criteria of high input impedance and low temperature operation as primary requirements, have led to the use of MOSFETS. Stability of operating parameters in the region of 4.2^{O}K led one investigator to use an electrometer vacuum tube, the Raytheon CK587, in preference to the MOSFET. Silicon junction FET devices exhibit low noise but will not operate below about 50^{O}K.

The literature contains information relative to a number of MOSFET devices. In addition, tests were conducted at the USU Electro-Dynamics Laboratories on four representative devices: the Texas Instruments Germanium FET type TIXM301, the Raytheon electrometer vacuum tube type CK587, the Silconix silicon junction FFT type 2N5199 and the Burr-Brown 3521R integrated operational preamplifier which contains selected 2N5199 type JFET input devices. Table 2 gives the results of a room temperature short circuit noise test on these devices which shows the superiority of the silicon junction FET in both absolute and 1/f noise voltage.

The ac gain of the electrometer tube, and the MOSFETS connected in a follower circuit varies from 0.1 to 0.3 which means that the effective noise is considerably larger than that indicated by the short-circuit noise measurement. The ac gain of the silicon JFET is very nearly unity at any temperature above 50^{O}K. The Burr-Brown integrated JFET-operational amplifier must be operated between 200 and 270^{O}K.

The Burr-Brown 3521R is utilized in the LSP-1 system which must be packaged in a special mount that provides:

(1) An operational temperature of 200^{O}K and which provides adequate insulation to prevent an excessive heat input to the dewar cold finger.

(2) Shield the detector from the 3521R thermal emissions.

TABLE II

Short Circuit Noise Voltage of Preamplifier Active Devices

Device	Noise Voltage (rms/Hz x 10^{-9}) 20 Hz	100 Hz	300 Hz
3521R		25	
2N5199	50	38	26
TIXM301	300	130	75
CK587	500	230	150

(3) Hold the 3521R and associated thermally insulating leads so that no microphonic generating motion is possible.

(4) Provide a very short lead wire between the device input gate, the detector, and the feedback resistor to reduce lead capacitance.

The 3521R will go into a pinch off condition if it is allowed to cold soak in an off mode. To restore normal operation it is necessary to apply heat to bring the temperature up to an operating level. The heater consists of a resistor that is heat sinked to the TO-99 package of the 3521R. A temperature sensing diode is mounted with the heater and is connected to an automatic control system that regulates the temperature at the required level.

The heater control circuit is a proportional system, so that once the 3521R reaches a temperature to permit normal operation, the self-heating effect will provide most of the heat input to maintain the system at $200^{O}K$.

The preamplifier provides compensated or uniform response as a function of frequency. That is, all the time constants associated with this circuit are reduced by the open loop gain of the amplifier.

The detector noise (photon noise) and the signal roll-off at 6-decibels per octave above the break frequency which is determined by the preamplifier input capacitance. This frequency response roll-off can be compensated to produce a flat (i.e., uniform) response as a function of frequency without changing the signal to noise ratio. The conventional method to achieve this flat response is to use a bridge bias network followed by an equilization amplifier.

However, the TIA preamplifier provides compensation through the use of negative feedback that results in the so-called virtual ground at the

input. The virtual ground produces other desirable effects in the TIA circuit that are not present in an equilization amplifier, they are

(1) Linearity. The detector is operated in a short circuit current mode that results in constant bias regardless of signal level, so long as the preamplifier is not saturated.

(2) Cross talk. The signal voltage appearing across the detector is reduced by a factor equal to the open loop gain of the preamplifier, a direct consequence of the virtual ground. In a multi-element detector array the cross talk is reduced by the product of the open loop gain of the channels.

(3) Microphonics. The input capacitance behaves as a capacitive microphone. Every effort must be made to rigidify the leads to reduce such effects. The virtual ground, in effect produces a low impedance short-circuit across that capacitance, reducing the microphonics by a factor equal to the reciprocal of the preamplifier open loop gain.

The operation of liquid-helium cooled extrinsic detectors, at reduced background results in "enhanced" operation. The relative ability to detect low-level incident radiation is improved and the detector impedance becomes very high. These effects result from the reduction of the background to essentially zero levels when cooled to near liquid-helium temperatures.

Under low background conditions the most significant detector parameter is the responsivity defined as the ratio of the current (or voltage) output to the radiant power input. The limiting noise is system generated noise because photon noise in the detector is essentially nonexistant at $20^{o}K$ or less. Thus, the noise equivalent power (NEP) for such a detector is

$$\text{NEP} = \frac{P_i}{\text{SNR}} = \frac{P_i e_n}{e_s} = e_n/R \qquad (1)$$

where

P_i is the incident power (watts)

e_n is the system noise (rms-volts)

e_s is the signal voltage (rms-volts)

R is the responsivity (rms-volts per watts)

SNR is the signal-to-noise ratio

These high impedance detectors actually behave very nearly as ideal current sources. The transfer impedance feedback resistor converts the output current to a voltage. Thus, the responsivity R_i of Equation (1) is the product of the current responsivity R with the value of the feedback resistor R_f.

The ultimate enhancement is obtained at very low frequencies where the limiting noise voltage is the feedback resistor thermal noise given by the Johnson-Nyquist equation

$$e_j = (4kTR_f \Delta f)^{\frac{1}{2}} \qquad (2)$$

where

k is Boltzmann's constant ($1.38 \times 10^{-23} J {}^{o}K^{-1}$)

T is the absolute temperature (^{o}K)

R_f is the feedback resistor (ohms)

Δf is the noise bandwidth (Hz)

At these low frequencies the ultimate value of NEP is given by

$$\text{NEP} = \frac{(4kT\ \Delta f)^{\frac{1}{2}}}{R_i (R_f)^{\frac{1}{2}}} \qquad (3)$$

Equation (3) illustrates that minimum NEP is obtained by reducing the temperature T of the feedback resistor, and by making R_f as large as possible. Values of R_f as high as 10^{11} ohms, cooled to near helium temperatures, are used in practice. The detector figure of merit D* does not apply in this case since the limiting noise is independent of the detector area.

For a thermal noise limited system the noise and signal roll-off at 6-decibels per octave above the break frequency; consequently, the SNR is constant and Equation (3) is valid except above some relatively high frequency at which the thermal noise is less than the preamplifier noise. At this frequency and for higher frequencies the SNR and NEP deteriorate at 6-decibels per octave.

Instantaneous preamplifier output noise e_{on} is a function of the amplifier short circuit noise e_n, the input capacitance C_t, the chopping frequency f_c, and the feedback capacitance C_f, where

$$e_{on} = e_n \, jR_f(C_f + C_t)2\pi f_c + 1 \qquad (4)$$

Usually the quantity C_f can be neglected and then equation 3 is valid for the case where the preamplifier output noise is less than the resistor thermal noise,

$$e_n \left| \; j2\pi f_c R_f C_t + 1 \; \right| < \; 4kTR_f^{\,\frac{1}{2}} \qquad (5)$$

Thus the feasibility of large R_f values and the resultant low values of NEP depend directly upon the value of the short circuit noise voltage and the input capacitance C_t of the electrometer preamplifier.

The value of R_f (cold) used for the low background conditions is 1.5×10^{10} ohms which result in a bandwidth of dc to about 100 Hz without excess noise.

MASS SPECTROMETER DETERMINATION OF OZONE

Optical Calibration System for Ozone

A spectrophotometer was specially designed and constructed to determine ozone concentration. Instead of the conventional dual beam system with separate monochromatic beams traversing each of two identical absorption cells, a single cell was used with both the sample and the reference beam alternately traversing the cell. The sample beam wavelength of 255 nm was chosen so as to correspond with the maximum of the Hartley absorption band. A reference beam of 400 nm was obtained using a narrow band filter as a beam splitter. The extinction coefficient at 400 nm is at least five orders of magnitude less than that at 255 nm. A diagram of the system is presented in Figure 6.

The hydrogen lamp and housing used in the spectrophotometer were obtained from a Beckman DU Spectrophotometer. Prior to entering the monochromator, the light beam is separated by the narrow band filter. The filter is designed to transmit 434 nm light, but the transmitted wavelength depends on the angle of incidence. With the filter placed at a 45^{o} angle to the incoming beam, the wavelength of the transmitted light is 400 nm. The remaining light is reflected to the monochromator where the sample beam is obtained. The intensity of the reference beam is adjusted by a variable slit as it is reflected around the monochromator. A lense in this region projects an image of the variable slit on the vibrating mirror between the monochromator and the absorption cell. A front-surface mirror attached to one tong of a tuning fork (100 Hz) simultaneously reflects the reference beam through the absorption cell and chops the sample beam. The lense between the mirror and the absorption cell columnates the light beam.

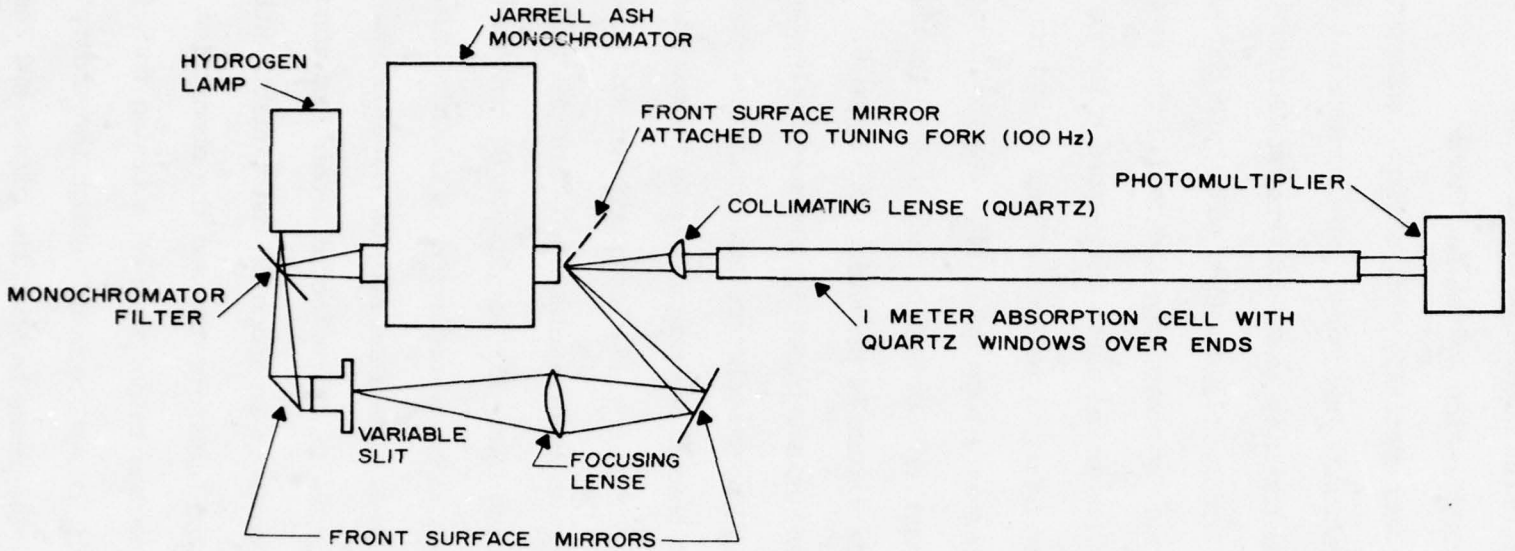

Figure 6. Ozone spectrophotometer, schematic diagram.

The absorption cell was constructed of pyrex tubing, the ends of which were covered with quartz plates. The 1-m tube was etched on the inside to minimize reflections. The light transmitted through the cell was monitored with a photomultiplier. The photomultiplier output was phase-sensitive amplified to detect slight differences between the two beam intensities. Differences corresponding to 10^{-4} of the unattenuated sample beam were repeatedly measured. This puts a sensitivity limit of approximately 20 ppb O_3 at atmospheric pressure. This limit was imposed by a sloping baseline at this sensitivity caused by intensity variations in the lamp emissions corresponding to the sample and reference wavelengths. If this problem could be remedied, the sensitivity could be increased by another order of magnitude. The optical system was calibrated against iodine vapor which has a broad absorption maximum at 500 nm and no absorption in the 400 nm region.

Mass Spectrometry

The mass spectrometer consisted of an EAI quadrupole mass analyzer updated by R.M. Jordan Co. The detector was a 14 stage Cu-Be electron multiplier and the ionizer was aligned axial to the inlet orfice and the mass analyzer. The output from the detector was measured directly by a Keithley Picoammeter or by a PAR HR-8 amplifier. In both cases, the field was swept over 2 amu and the difference signal (m/e 48 -m/e 47) was used for the measurement.

This section includes the results from the mass spectrometric calibration of ozone and a discussion of possible chemical interferences. Ozone was calibrated against argon for mass spectrometer partial pressures of ozone between 10^{-6} and 10^{-11} torr. The mass spectrometer sampled from a gas flow containing ozone and freon or oxygen. Nitrogen or argon was added to dilute the gas mixture. The ozone concentration was monitored with a dual beam spectrophotometer having a 1 meter absorption cell. The ampere output of the mass spectrometer was converted to first dynode amps and plotted against the ozone partial pressure. A similar procedure was followed monitoring argon (Figure 7).

The distances traveled by ions under the influence of the ion repeller voltage has been determined by plotting the experimentally measured time from ionization to detection against the inverse square root of the ion energy ($E^{-\frac{1}{2}}$) (Figure 8). Argon (m/e 40) was used to obtain this measurement. The time of flight can be expressed by

$$t = \left(\frac{ml^2}{2e}\right)^{\frac{1}{2}} \frac{1}{E^{\frac{1}{2}}}$$

where t is the time; m is the mass of the particle; l is the distance; and e is the charge of an electron. The slope of t vs $E^{-\frac{1}{2}}$ can be expressed

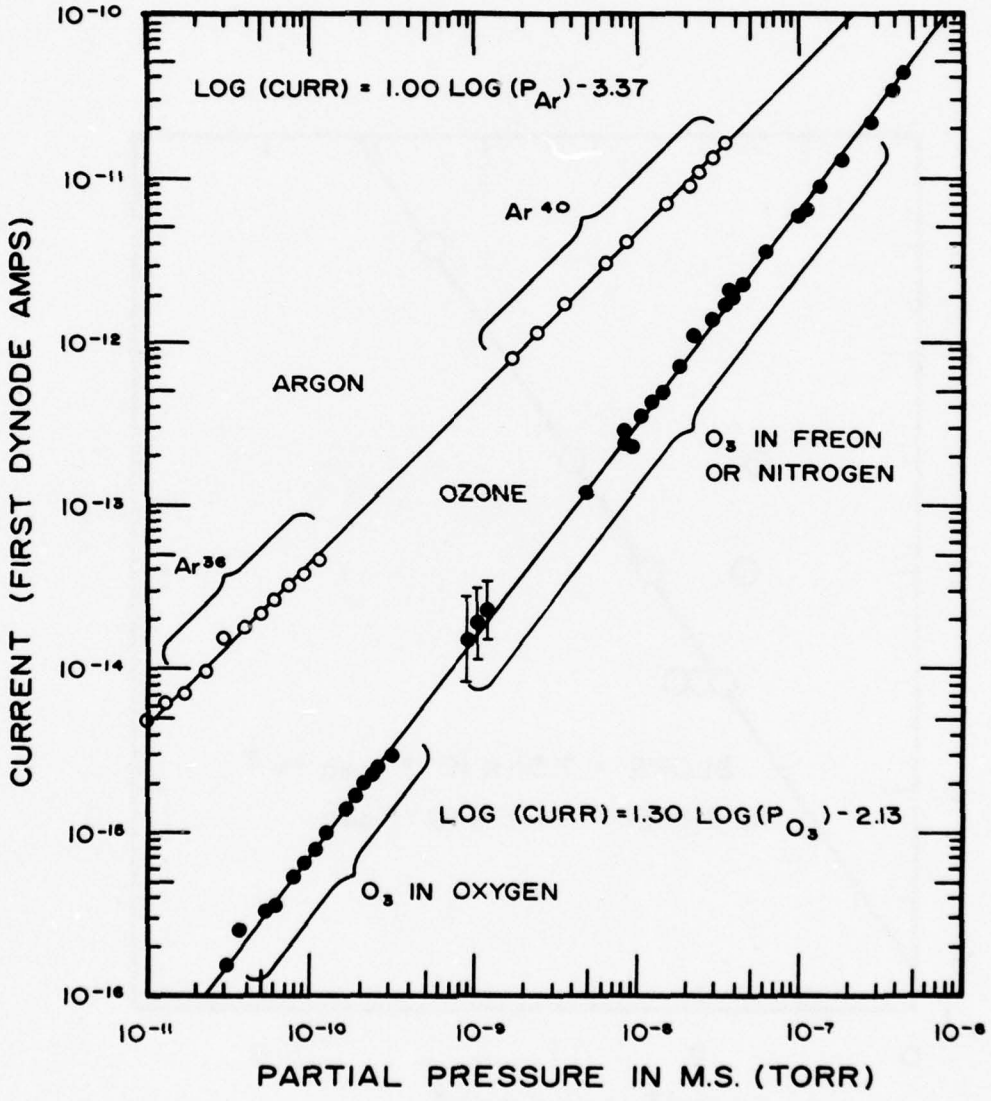

Figure 7. First dynode current as a function of the partial pressure of ozone and argon.

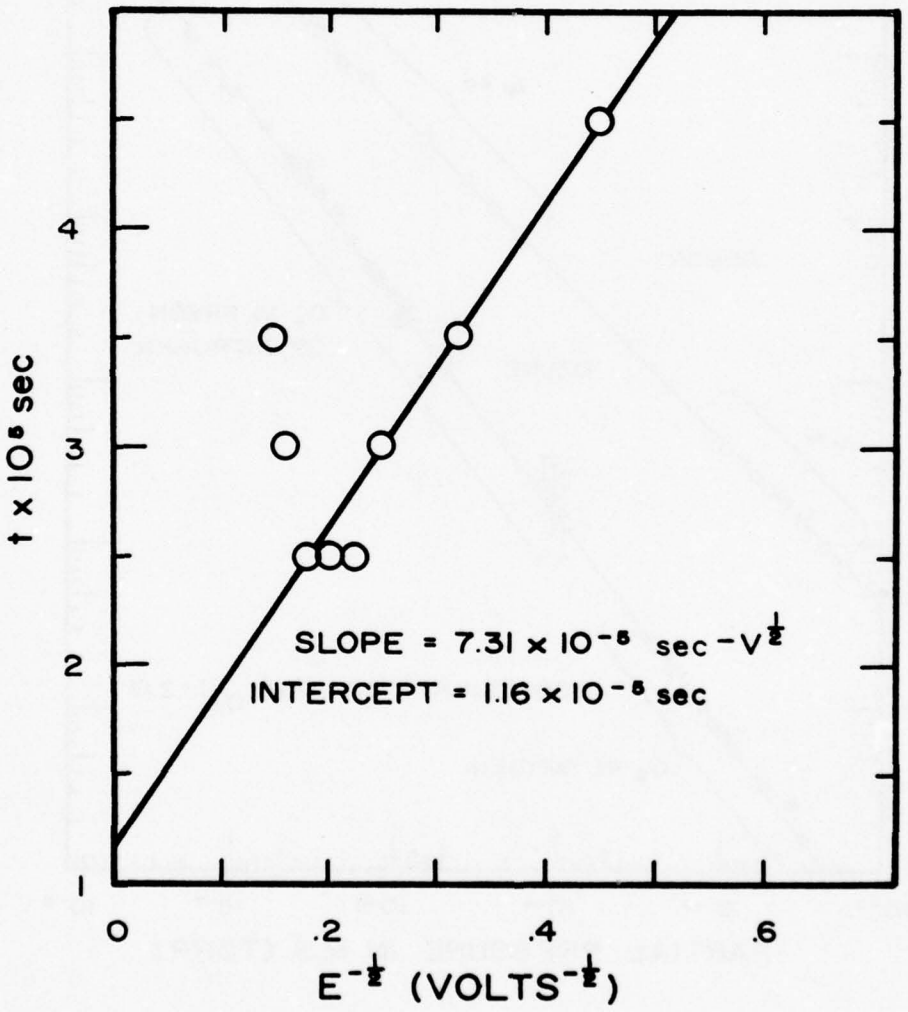

Figure 8. Drift time for positive ions in the mass spectrometer.

$$\text{slope} = \left(\frac{ml^2}{2e}\right)^{\frac{1}{2}}$$

The value calculated for l, 15.9 cm, is very close to the geometric measurement, approximately 16.5 cm. This experimentally measured distance (l) will be used for evaluating the possibilities for both unimolecular and bimolecular destruction of ozone. As is evident from Figure 2, there are deviations from the expected values at repeller voltages greater than 30 V. This probably due to a disturbance of the ionizing electron beam. The same observation is seen in the plots of signal intensity against ion energy, showing a maximum for both argon and ozone near 30 V ion energy (Figure 9).

The signal intensity as a function of ionizing electron energy has been determined for both ozone and argon. Both curves show the same general appearance, with argon having a maximum near 40 eV and ozone having a somewhat broader maximum near 50 eV. This can be expected, since ozone also contains vibrational energy levels which could allow a slightly larger range of energies to cause the same electronic transitions (Figures 10 and 11).

The ionization potentials for ozone and argon have been determined from these plots as 13 eV and 15 eV, respectively. Using the same method, values of 12.80 eV and 16.5 eV, respectively, were obtained previously (Herron and Schiff, 1956; Mathias and Schiff, 1964).

The importance of O_3^+ unimolecular destruction can be obtained by comparing O_3^+ signals to Ar^+ signals as a function of ion energies. Any unimolecular O_3^+ destruction will be dependent on the time between ionization and detection (an expression has already been given). Since Ar^+ has no means for unimolecular destruction and the ions are accelerated such that collisions with the walls will be prevented, a plot of the

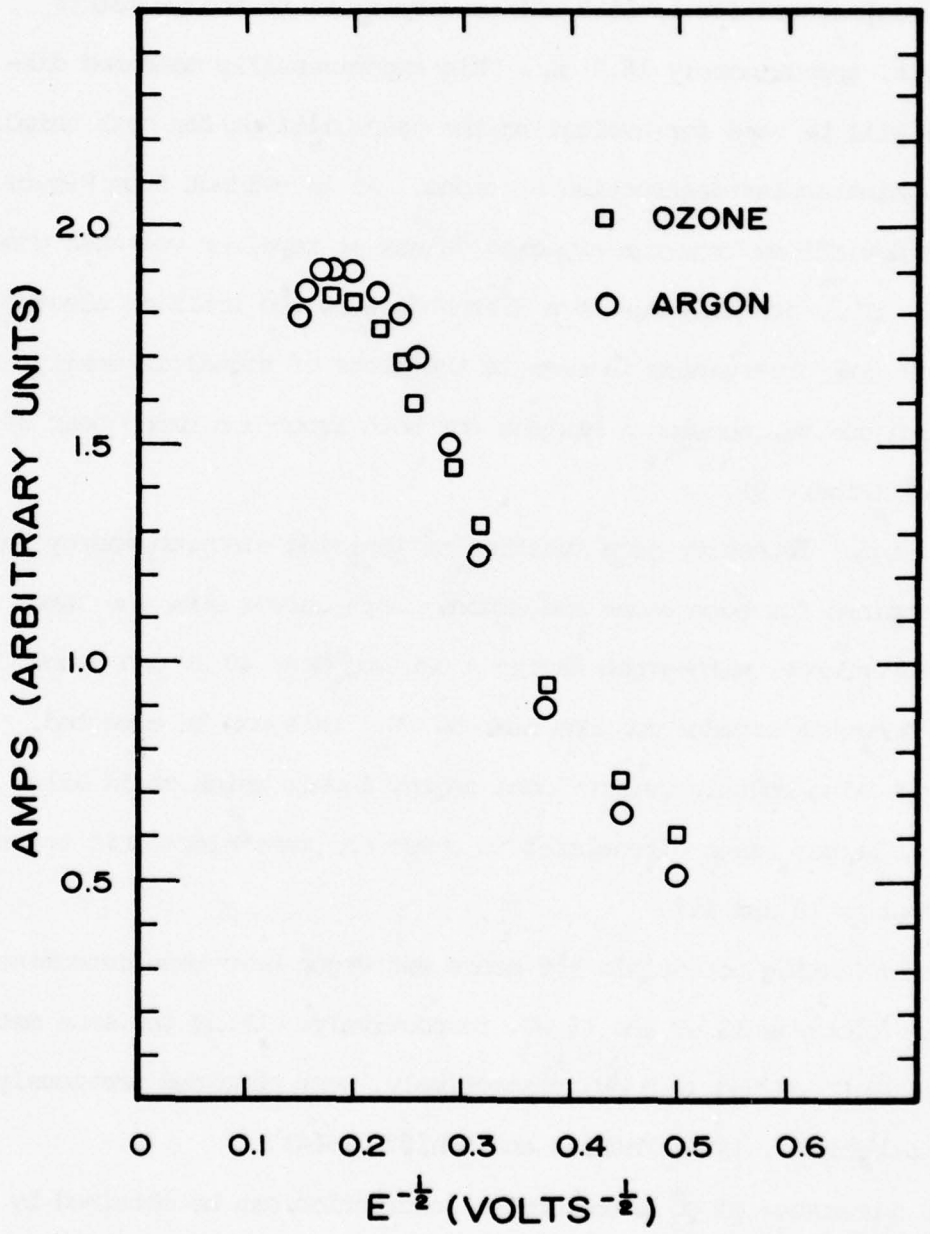

Figure 9. Signal intensity as a function of the ion energy.

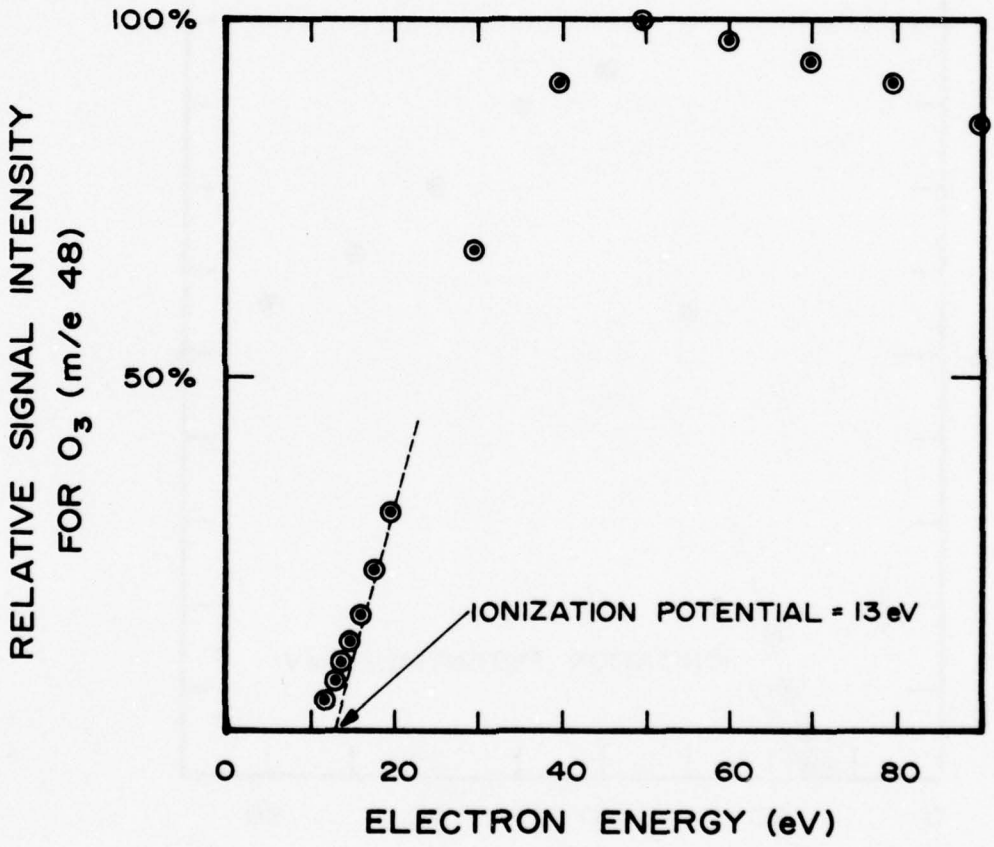

Figure 10. Signal intensity for ozone (m/e 48) as a function of electron energy.

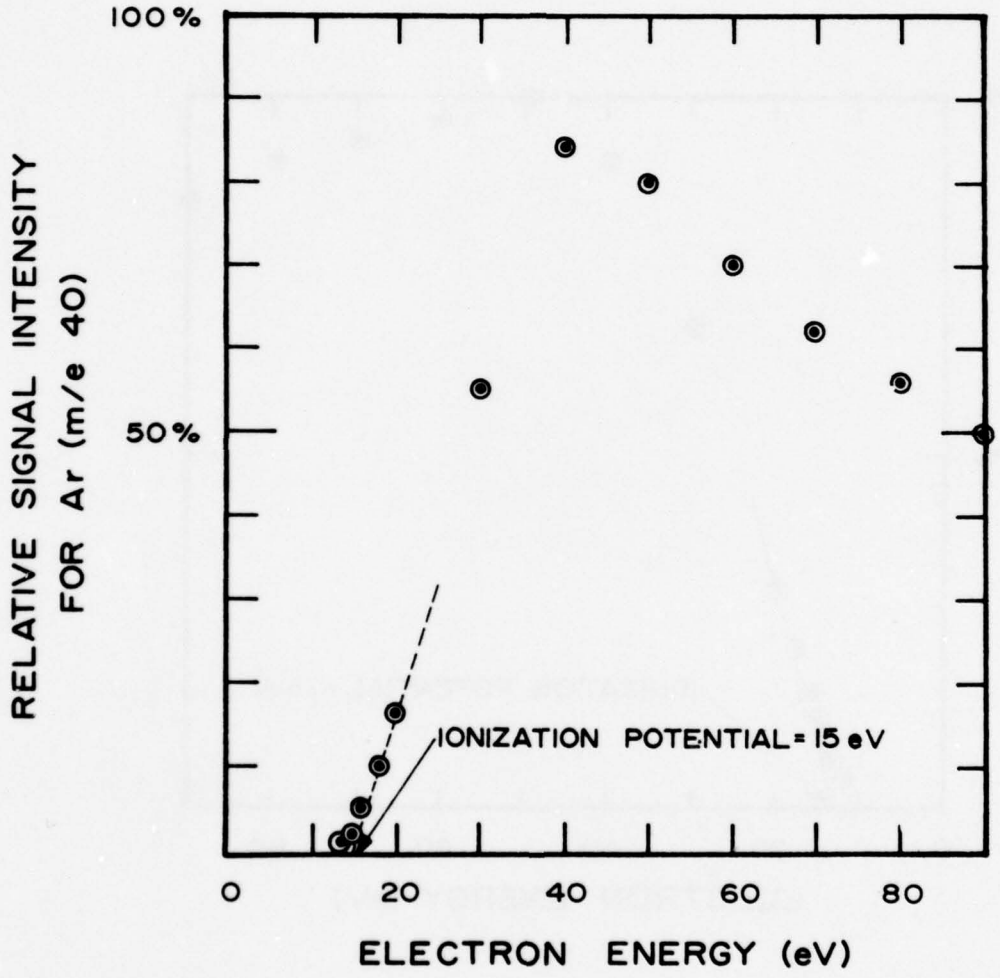

Figure 11. Signal intensity for argon (m/e 40) as a function of electron energy.

ratio O_3^+/Ar^+ against $E^{-\frac{1}{2}}$ should show a negative slope if this destruction is of importance and a slope of zero if it is not. From the data plotted in Figure 12, it can be concluded that the unimolecular destruction of O_e^+ will be negligible for the times between formation and detection of the ions in the mass spectrometer.

The fractional order dependence for O_3^+ formation indicates there must be an additional mechanism for either destruction or formation of O_3^+. The Langevin orbiting collision treatment

$$O_2 + O_3^+ \rightarrow O_2^+ + O_3 \qquad (1)$$

$$O_2^+ + O_3 \rightarrow O_3^+ + O_2 \qquad (2)$$

for either reaction (1) or (2) is given by

$$Q = 2\pi \left(\frac{\alpha e m_i}{2ME}\right)^{\frac{1}{2}}$$

where Q is the collision cross-section, α is the polarisability of the neutral molecule, m_i is the mass of the ion, M is the reduced mass of the collision pair, and E is the accelerating potential for the ion. With an ion energy of 15 volts, which was used for all sensitivity measurements, $Q_1 = 8.7\ \text{Å}^2$, and $Q_2 = 16\ \text{Å}^2$, for reactions (1) and (2), respectively. The fractional ion loss by this mechanism is then

$$\frac{i(new^+)}{i(parent^+)} = nlQ$$

where n is the number density of the neutral species, and l is the distance travelled by the parent ion. At a pressure of 4×10^{-6} torr. for O_2 containing 10% O_3, the fractional losses are 2×10^{-3} and 3×10^{-4} for reactions (1) and (2), respectively.

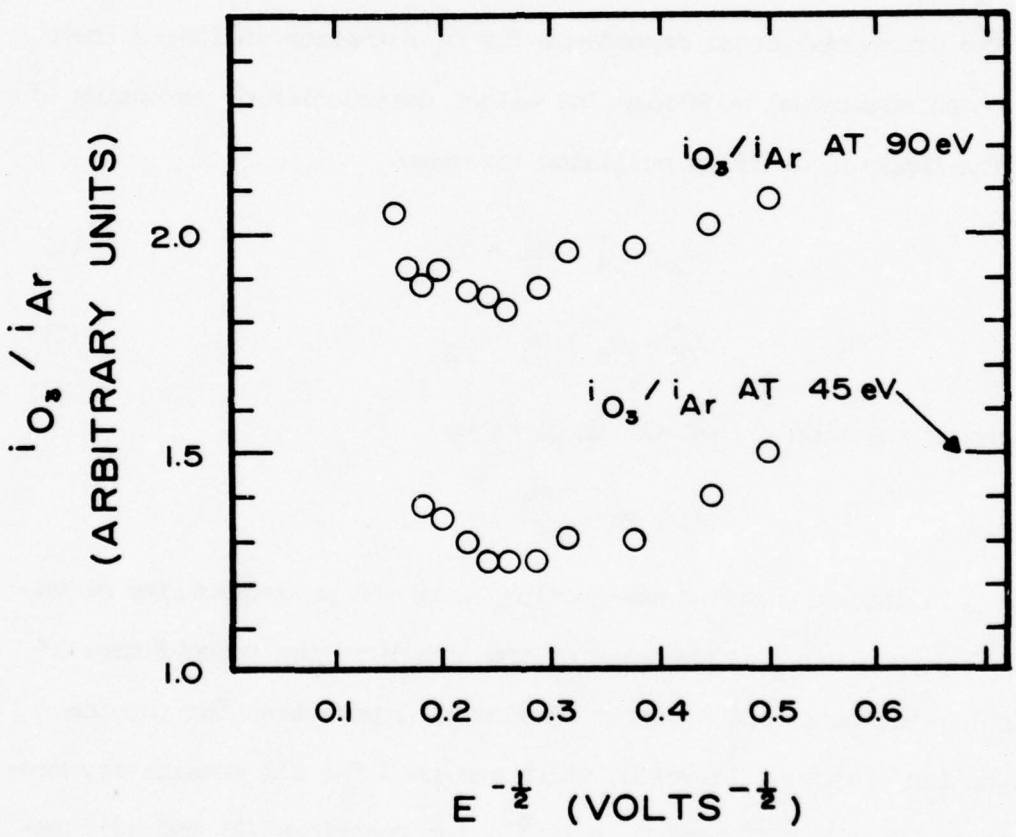

Figure 12. Ratio of O_3^+ to Ar^+ signal as a function of ion energy.

Since the total pressure was kept constant during all measurements, it seems clear that reaction (1) can have no noticeable detrimental effect on the yield of O_3^+. However, the enhancement of yield of O_3^+ by reaction (2) will be dependent on ozone concentration. The theoretical calculation of Q_2 would have to be low by a factor of almost 30 for the contribution of reaction (2) to dominate at the upper concentration range of O_3.

A final mechanism, which involves only ozone, has the same range of collision cross-sections as reactions (1) and (2) above.

$$O_3 \xrightarrow{e^-} O_3^+ \rightarrow O + O_2^+ \xrightarrow{O_3} O_3^+ + O_2$$

This sequence would appear bimolecular for O_3^+ formation. In the pressure region of our experiments any of these possibilities seem remote, but they have been observed at pressures 10^3 greater (Cook, 1968).

Summary of Ozone Detection by Mass Spectrometry

The optical system for the absolute measurement of ozone was calibrated against iodine vapor and the results were satisfying. The mass spectrometer including the inlet orfice was calibrated against the natural abundance of argon in air, and there were no anomolies found. The efficiency of the formation of O_3^+ in terms of Ar^+ was found to agree with Schiff and Phillips in the short concentration range covered by them. The pressure in the ionizer and mass spectrometer were lower by a factor of 100 than required to have ion-molecule interactions. The results still show that the efficiency of formation of the parent ion, O_3^+, is dependent on the pressure of ozone to the 1.3 power. This dependence extends over 5 magnitudes and it is independent of the nature of the carrier gas.

A modulated molecular beam apparatus would permit the detection of even lower partial pressures of O_3, but the extrapolated limit seems to be 10^{-13} torr. This means that parts per million of ozone could be detected at 10 torr external pressure, and parts per billion at 10^{-4} torr. However, it is unlikely that a satisfactory beam could be formed at 10^{-4} torr.

OXYGEN ATOM DETECTION WITH SILVER THIN FILMS

Molecular oxygen will not form an oxide with silver, but it will be absorbed as a surface layer (Czanderna, 1964). Silver is oxidized by atomic oxygen (Asakura, 1969; Wood, 1971), and silver also catalyzes the surface recombination of atomic oxygen to form molecular oxygen (Myerson, 1963; Sjolander, 1976). The oxidation of thin silver films has been the basis of a detector system to monitor atomic oxygen concentrations in the upper atmosphere (Thomas, Henderson, Henderson and Schiff). The changing resistance of the film as its composition changed from pure metal to silver oxides was employed as a calibrated measure of the integrated atomic oxygen exposure. Most of the studies cited have used some indirect method to measure the chemical transformation. We have studied the oxidation of silver thin films by following the mass change of the film.

Experimental

Thin Film Formation

Thin silver films, 10 to 100 nm thick, were vacuum deposited at less than 10^{-6} torr over a 100 nm layer of gold that had been deposited on a substrate of polished AT cut quartz wafer. The deposition rate was 0.8 nm/sec as determined by a Kronos QM-1 Digital Thickness Monitor. This produced a film which had a large number of small islands and greater structural defects (Chopra and Randlett, 1968), and the crystal orientation is along the 111 plane (Dobrev, 1974). Both the quartz wafers and glass microscope slides were cleaned for deposition by; (1) an ultrasonic bath containing Miro solution for 15 min., (2) rinsed with distilled water, (3) rinsed with distilled water in the ultrasonic bath for 5 min., (4) rinsed with deionized water in the ultrasonic bath twice, (5) placed in metal holders wet, and (6) dried in an oven at 105^{o}C for at lea t one hour. The finished silver films were stored in an airtight container filled with dry nitrogen until used.

Several experiment were performed with the silver film deposited on glass microscope slides. For resistance measurements on the silver film during oxidation, wires were connected to the glass and coated with conducting silver paint as described by Thomas and Baker (1970).

Apparatus

Atomic oxygen was generated by flowing nitrogen through a microwave discharge and titrating the nitrogen atoms with nitric oxide to form atomic oxygen. By this procedure no electronically or vibrationally excited oxygen was produced and only a small amount of nitric oxide was present which has been shown to be inert to silver films. The measured

flow of nitric oxide was used to determine the oxygen atom concentration (Kaufman, 1958; Westenberg and de Haas, 1964). At low concentrations many oxygen atoms were lost due to recombination even though the glass vacuum system was coated with phosphoric acid. The atomic oxygen concentration was finally calibrated by titrating the oxygen atoms with NO_2 after the reaction chamber. The complete arrangement is shown diagrammatically in Figure 13. The titration to form atomic oxygen was performed automatically by monitoring the chemiluminescence of NO_2 produced in the slow reaction of O + NO at the end point.

The silver films were placed in the reaction chamber on an appropriate holder joined to a ground glass joint. The holder had many shapes, but for mass change measurements, it consisted of the transducer element of a Kronos QM-311 Digital Thickness Monitor sealed into the glass joint. The exposed metal retainer ring for the quartz crystal was teflon coated to reduce surface recombination in the vicinity of the silver film.

Detection Systems

The mass gain of the silver film was followed using the Kronos QM-311 DTM. The response of the instrument is 1×10^{-8} g-cm^{-2}-count^{-1} or 3.76×10^{14} O atoms-cm^{-2}-count^{-1}. The use of AT-cut quartz crystals minimizes the thermal response of the instrument, and the frequency instability in the temperature range (17-40C) is 10 ppm (Heising, 1946). The transducer element was temperature controlled during the rate measurements. The instrument was calibrated by depositing gold on an accurately measured surface and weighing the deposit with a microbalance. This calibration agreed with the instrument specifications to within the experimental error of 1%.

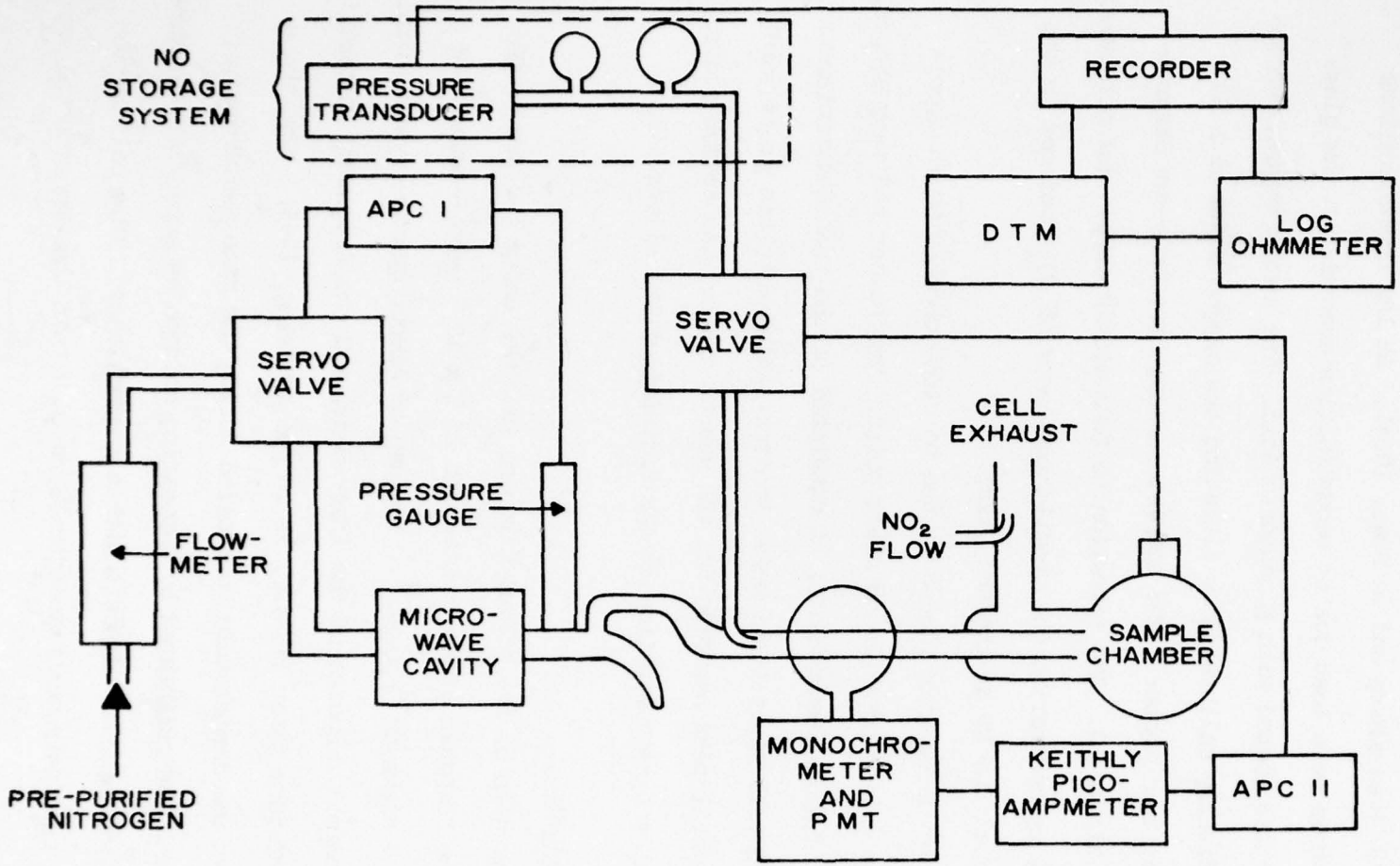

Figure 13. Functional diagram of atomic oxygen vacuum system.

The X-ray diffraction spectra were taken with a Seimens Kristalloflex 4 equipped with a 35 kV, 18 ma, copper X-ray tube. All spectra were taken at a speed of 1 Bragg angle per minute and they were recorded on a strip chart recorder.

The thermal decomposition studies were performed in a glass oven attached directly to a quadrupole mass spectrometer. The oven was at the same pressure as the mass spectrometer. A Chromel-Alumel thermocouple was sealed into the oven to make good thermal contact with the silver film and crystal.

Results

A plot of the mass gained during an oxidation, versus time is shown in Figure 14. Three portions of the oxidation curve which represent different oxidation processes are indicated on the figure. Kinetics studies have been completed on the initial rate and the post-AgO rate. The initial formation of AgO has been substantiated by X-ray diffraction spectra of the oxidized films and a plot of the mass gained to the first major slope change (Figure 15). The overshoot of the stoichiometric ratio is due to the post-AgO oxidation. The data pictured in Figure 15 were all obtained from oxidations at 25°C. If the temperature is increased to 40°C, the lines coincide. The post-AgO oxidation is essentially stopped at 40°C. An analysis of the zero order rate constants for this portion of the curve yields an Arrhenius activation energy of -13 kcal/mole.

The kinetics study of the initial zero order rate showed a first order dependence on the concentration of atomic oxygen. The first order rate constant was determined to be 13 cm/sec. There was no correlation between the rate and either oxidation temperature or film thickness over the ranges studied, 15 to 40°C, and 100 to 750 Å.

Thermal decompositions coupled with a determination of the emitted oxygen yielded conformation of the initial formation of AgO. The decomposition curve, shown in Figure 16, exhibits two major peaks, one at 110°C and the other at 250°C. The peaks are of approximately equal area. The first peak is the decomposition of AgO to Ag_2O, which then decomposes at the higher temperature. The low temperature decompositions, just above room temperature, are the decompositions of the loosely held atomic oxygen in the AgO. Evidence has been observed, indicating that atomic

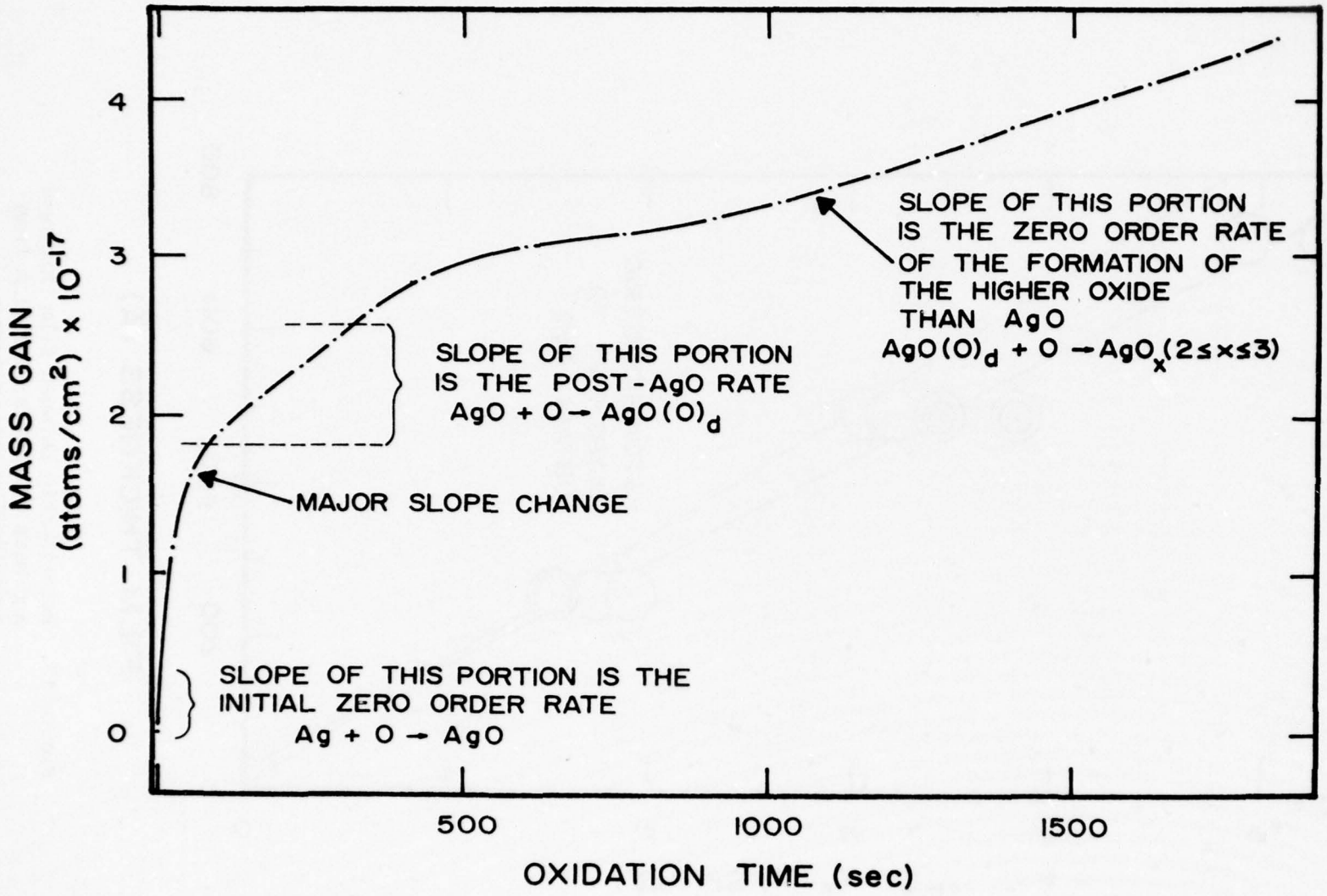

Figure 14. Mass gain of silver film as a function of oxidation time.

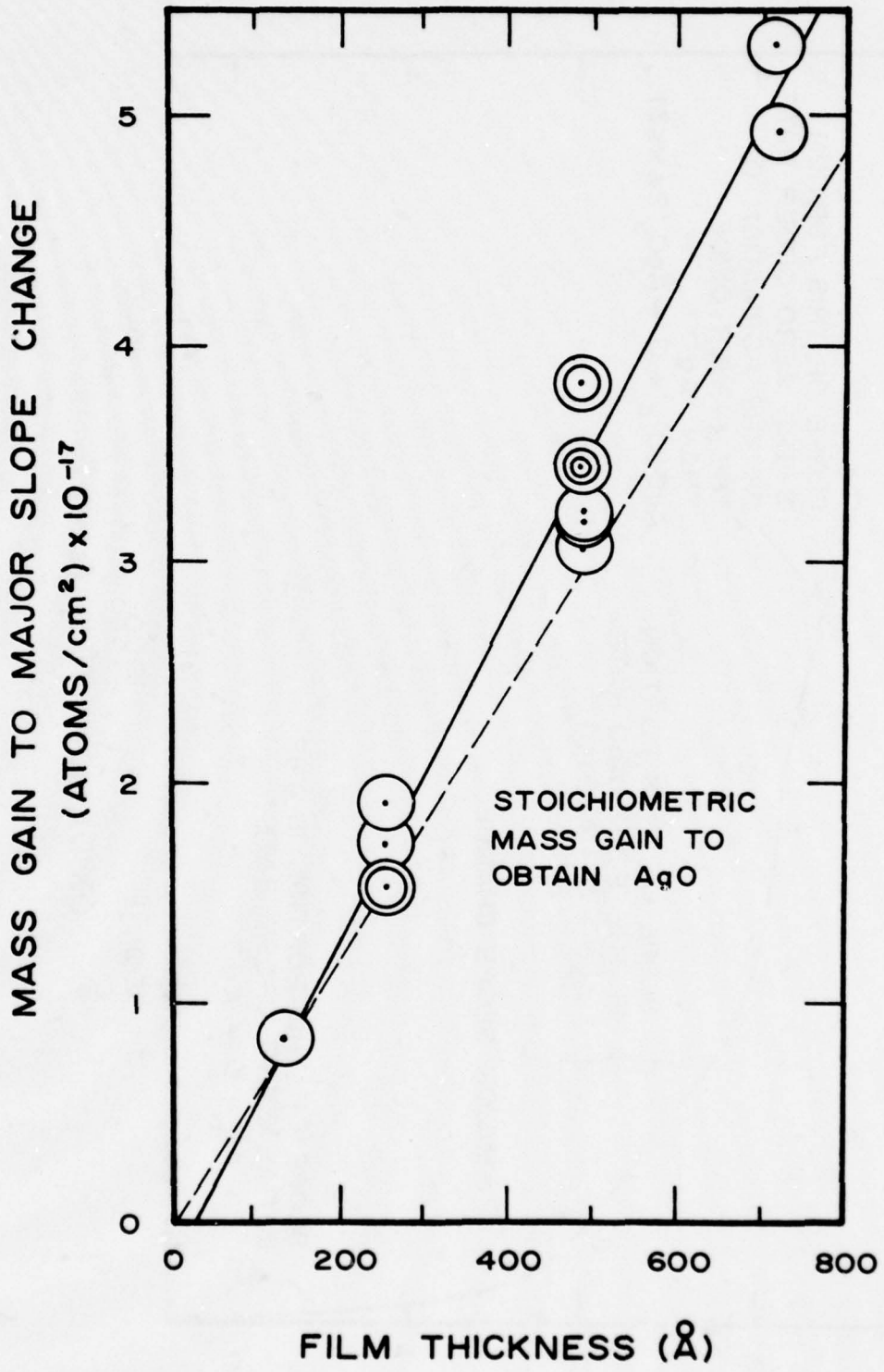

Figure 15. Relationship between film thickness and mass gain of silver film from oxidation by atomic oxygen.

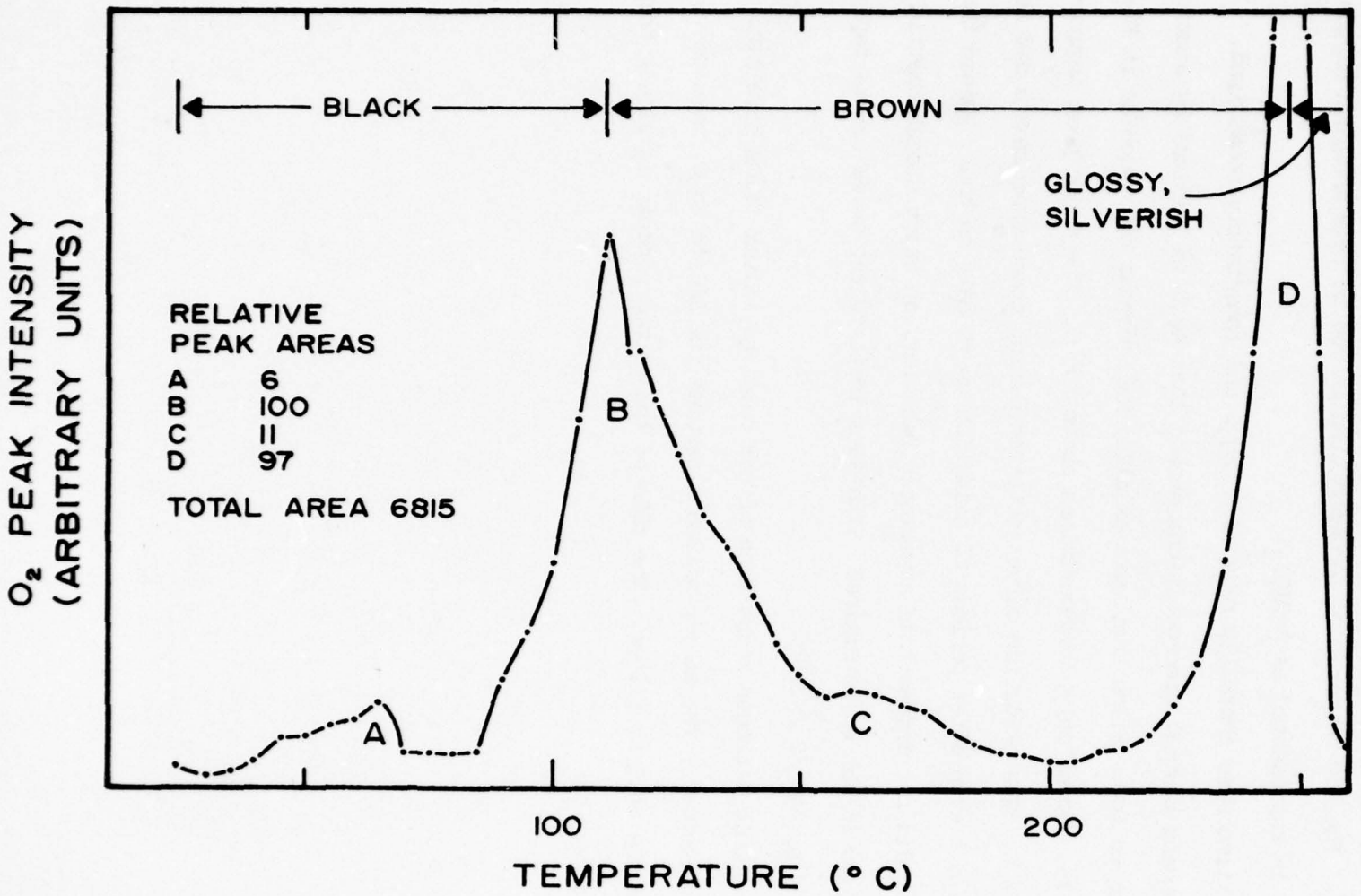

Figure 16. Temperature dependence for the decomposition of the silver oxides formed on silver film.

oxygen is able to penetrate the AgO lattice for distances of at least 1000Å. The low temperature decomposition is due to this absorbed oxygen, which is represented as $AgO(O)_d$.

Films were thermally reduced to Ag_2O and immediately reoxidized. Subsequent thermal decompositions showed that Ag_2O is oxidized by atomic oxygen to AgO. Films that were oxidized well beyond AgO, such as in Figure 15, showed only decompositions above 300°C. The major peak occurred at 350°C. The oxidation curves obtained during these experiments did not level off even after periods of oxidation up to half an hour. Since the curves did not demonstrate asymptotic behavior, an exact stoichiometric ratio could not be determined. The data indicate the oxide can be represented by $AgO_x (2 \leq x \leq 3)$.

Atomic nitrogen reductions of the oxidized silver films have also been observed. The atomic nitrogen reduces the AgO to Ag_2O, then reduces the Ag_2O to silver. The rate of the second process is slower than the first.

Conclusions

The oxidation of silver by atomic oxygen has been shown to produce AgO. The initial rate demonstrates first order kinetics with respect to the concentration of atomic oxygen. Continued oxidation produces higher oxides with the initial step being the formation of an intermediate designated $AgO(O)_d$. This process has a large negative Arrhenius activation energy, -13 kcal/mole, and is essentially stopped at 40°C. This species also decomposes to Ag_2O, even at room temperature. The behavior of this species is similar to that attributed to AgO by Myerson (7) in the formulation of his mechanism for surface recombination An alternate mechanism would propose the initial formation of AgO followed by the oxidation to a higher oxide, which then reacts with atomic oxygen, liberating molecular oxygen:

$$Ag + O \rightarrow AgO$$

$$AgO + O \rightarrow AgO(O)_d$$

$$AgO(O)_d + O \rightarrow AgO + O_2\uparrow$$

After the formation of the intermediate, oxidation to a higher oxide proceeds. The formula for the higher oxide cannot be identified exactly but is approximated by the relationship,

$$AgO_x (2 < x < 3).$$

This is definitely a stable compound, as indicated by the high temperature of the thermal decomposition peak, higher than either of the other known silver oxides. The pathways between the different silver oxides and intermediates are pictured in Figure 17.

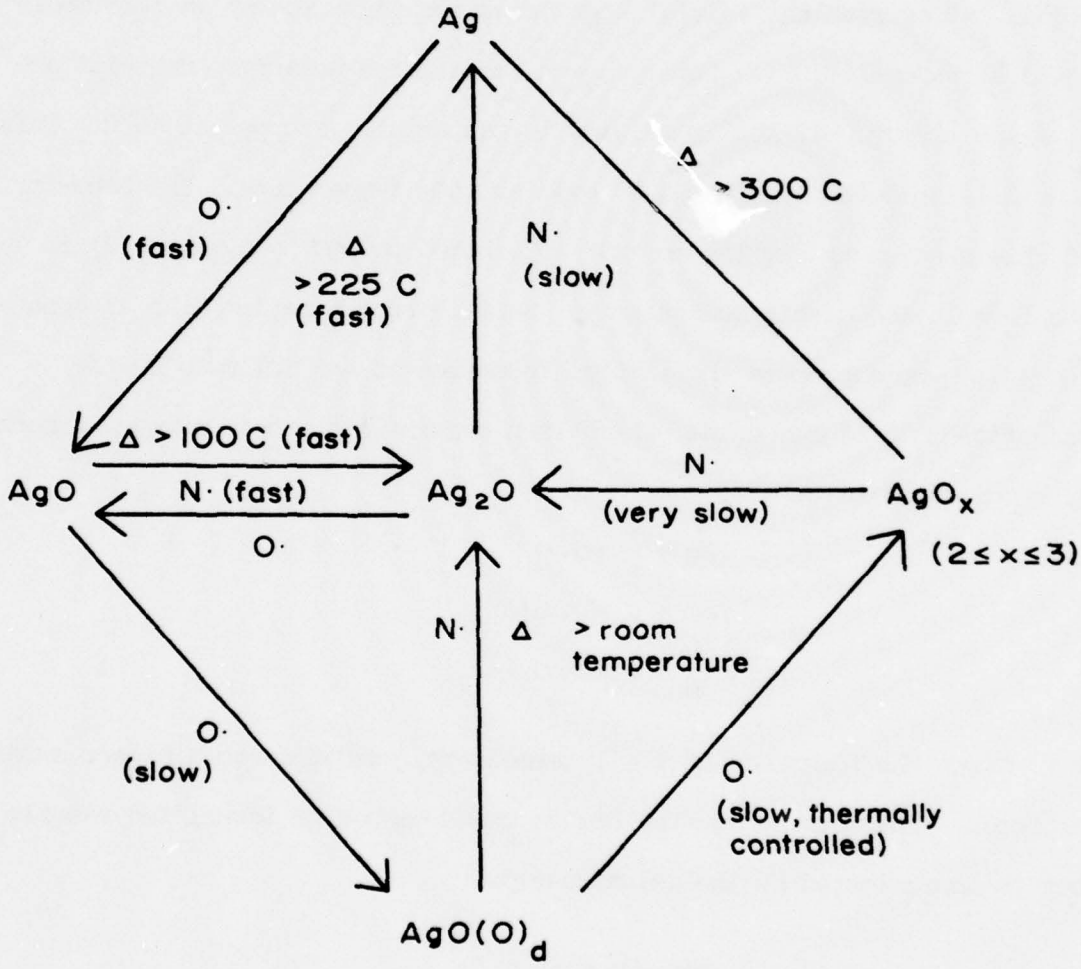

Figure 17. Proposed mechanism for the oxidation and reduction of silver thin films.

Evidence demonstrating that resistance is a poor method to monitor the extent of oxidation was also obtained. The resistance has been shown to depend upon the properties of each individual film. This explains the difficulties encountered by previous workers with their atmospheric detector (6). An alternate method, the surface reflection of light, appears to be a new technique for monitoring the oxidation of silver films. A light beam is reflected off a silver surface, shining on a detector. As the surface is oxidized, the intens ty of light reaching the detector diminishes. Preliminary experiments have shown this method to be quite sensitive, giving results comparable to the mass gained during early oxidation stages. Using a double beam reflectivity measurement, a partial pressure of O atoms of 10^{-5} torr could be detected (3×10^{10} atoms/cc). This method would be useful for an atmospheric measurement of O atoms at 60-100 km.

NEGATIVE SURFACE IONIZATION FOR THE DETECTION OF OZONE

The interferences produced by oxygen in the positive ion mass spectrometric analysis of ozone, and the nonlinear response of O_3^+, made us examine other possible mass spetrometric methods. The principal fragments from ozone are at m/e 32 and m/e 16, and both peaks are completely masked by trace amounts of O_2 in the analyzed gas.

Negative surface ionization (NSI) of gases has been examined for a few materials, and most of the work was done with carbon tetrachloride (Persky et al, 1968; Cardillo et al, 1971). Two criteria were developed on the basis of these early studies; (1) the filament material must have a low work function (i.e., it must release electrons easily at relatively low temperatures), and (2) the gas must have a high electron affinity (i.e., it must be available for the attachment of an electron). The best filament material found so far is niobium. It is not the most sensitive for CCl_4, but it has good long-term stability and it has the fastest relaxation time for the release of negative ions.

Using the expertise in mass spectrometry developed under this project, we modified the mass spectrometric apparatus to detect with separate mass analyzers both positive ions generated by electron impact, and negative ions generated by NSI. Also, the vacuum apparatus was rebuilt into a two chamber modulated molecular beam system.

The NSI apparatus has worked remarkably well and considerable data has been collected. Chlorine containing compounds have high sensitivity for NSI, but ozone has not been detected by the method up to the end of this contract. However, there is still a possibility for a successful measurement of ozone by this technique.

It seems that a third condition which applies to NSI is that the molecules must have a low threshold for electron attachment. Ozone has both a high electron affinity and a low threshold for electron attachment. Oxygen does not meet either condition and no signal is observed with oxygen as a carrier gas, but the filament forms an oxide layer which reduces its sensitivity by a factor of two. Carbon dioxide does have a high electron affinity, but it also has a high threshold for electron attachment and no signal is observed.

The NSI mass spectrum of clean air (N_2, O_2, CO_2, H_2O, and rare gases) is nonexistent. The major components of air or any normal carrier gas produce no interfere ces for NSI mass spectrometry. Upon electron attachment, ozone should fragment into O^- and O_2^- and no O_3^- should be observed.

Recently, we have found that the temperature of the filament is very sensitive to different elements, and each element has an optimum temperature for sensitivity and time retention on the filament. Ozone is the only substance predicted to have a NSI spectrum, and a negative result found. We suspect that the correct conditions have not been determined.

REFERENCES

Asakura, Y., *Nippon Kagaku Zasshi, 90,* 987 (1969).

Bennett, H.E., R.B. Peck, D.K. Burge, and J.M. Bennett, *J. Applied Phys., 40,* 3351 (1969).

Cardillo, M.J., M.J. Chou, E.F. Greene, and D.B. Sheen, *J. Chem. Phys., 54,* 3054 (1971).

Chopra, K.L., and M.R. Randlett, *J. Applied Phys., 39,* 1874 (1968).

Cook, G.R., *Trans. Am. Geophys. Union, 49,* 736A (1968).

Czanderna, A.W., *J. Phys. Chem., 68,* 2765 (1964).

DelGreco, F.P., J.P. Kennealy, F.X. Robert, and G.E. Caledonia, Abstract 173 Amer. Chem. Soc. Meeting (1977).

Heising, R.A., *Quartz Crystals for Electrical Circuits,* D. Van Nostrand Co., New York (1946).

Herron, J.T., and H.I. Schiff, *J. Chem. Phys., 24,* 1266 (1956).

Henderson, W.R., *J. Geophys. Res., 76,* 3166 (1971).

Kennealy, J.P., F.P. DelGreco F.X. Robe t, A. Corman, and W.M. Moore, Abstract, 173 Amer. Chem. Soc. Meeting (1977).

Kaufman, F., *J. Chem. Phys., 28,* 352 (1958).

Mathias, A., and H.I. Schiff, *Disc. Faraday Soc., 37,* 38 (1964).

Myerson, A.L., *J. Chem. Phys., 38,* 2043 (1963).

Myerson, A.L., *J. Chem. Phys , 42,* 3270 (1965).

Persky, A., E.F. Greene, and A. Kupperman, *J. Chem. Phys., 49,* 2347 (1968).

Sjolander, G.W., *J. Geophys. Res., 81,* 3767 (1976).

Thomas, R.J., and D.J. Baker, *Canad. J. Phys., 50,* 1676 (1972).

Westenberg, A.A., and N. Deltass, *J. Chem. Phys., 40,* 3087 (1964).

Wood, B.J., *J. Phys. Chem., 75,* 2186 (1971).

APPENDIX A

DISTRIBUTION LIST

DISTRIBUTION LIST

DIRECTOR
DEFENSE ADVANCED RSCH PROJ AGENCY
ARCHITECT BUILDING
1400 WILSON BLVD.
ARLINGTON, VA 22209
ATTN LTC W A WHITAKER

DIRECTOR
DEFENSE ADVANCED RSCH PROF AGENCY
ARCHITECT BUILDING
1400 WILSON BLVD.
ARLINGTON, VA 22209
ATTN MAJOR GREGORY CANAVAN

DEFENSE DOCUMENTATION CENTER
CAMERON STATION
ALEXANDRIA, VA 22314
ATTN TC

DEFENSE DOCUMENTATION CENTER
CAMERON STATION
ALEXANDRIA, VA 22314
ATTN TC

DIRECTOR
DEFENSE NUCLEAR AGENCY
WASHINGTON, DC 20305
ATTN RAAE CHARLES A BLANK

DIRECTOR
DEFENSE NUCLEAR AGENCY
WASHINGTON, DC 20305
ATTN TITL TECH LIBRARY

DIRECTOR
DEFENSE NUCLEAR AGENCY
WASHINGTON, DC 20305
ATTN TITL TECH LIBRARY

DIRECTOR
DEFENSE NUCLEAR AGENCY
WASHINGTON, DC 20305
ATTN TISI ARCHIVES

DIRECTOR
DEFENSE NUCLEAR AGENCY
WASHINGTON, DC 20305
ATTN RAEV HAROLD C FITZ, JR

DIRECTOR
DEFENSE NUCLEAR AGENCY
WASHINGTON, DC 20305
ATTN RAAE MAJ. J. MAYO

DIRECTOR
DEFENSE NUCLEAR AGENCY
WASHINGTON, DC 20305
ATTN RAAE G. SOPER

DIRECTOR
DEFENSE NUCLEAR AGENCY
WASHINGTON, DC 20305
ATTN MAJOR R. BIGONI

DIR OF DEFENSE RSCH & ENGR
DEPARTMENT OF DEFENSE
WASHINGTON DC 20301
ATTN DD/S&SS (OS) DANIEL BROCKWAY

DIR OF DEFENSE RSCH & ENGR
DEPARTMENT OF DEFENSE
WASHINGTON, DC 20301
ATTN DD/SS&SS DANIEL BROCKWAY

COMMANDER
FIELD COMMAND
DEFENSE NUCLEAR AGENCY
KIRTLAND AFB, NM 87115
ATTN FCPR

CHIEF LIVERMORE DIVISION
FLD COMMAND DNA
LAWRENCE LIVERMORE LAB
P.O. BOX 808
LIVERMORE, CA 94550
ATTN FCPRL

COMMANDER/DIRECTOR
ATMOSPERIC SCIENCES LABORATORY
U S ARMY ELECTRONICS COMMAND
WHITE SANDS MISSILE RANGE,NM 88002
ATTN DRSEL-BL-SY-A F. NILES

COMMANDER/DIRECTOR
ATMOSPHERIC SCIENCES LABORATORY
U S ARMY ELECTRONICS COMMAND
WHITE SANDS MISSILE RANGE,NM 88002
ATTN H. BALLARD

COMMANDER
HARRY DIAMOND LAB
2800 POWDER MILL RD
ADELPHI MD 20783
ATTN DRXDO-NP, F.H. WIMINETZ

COMMANDER
U S ARMY NUCLEAR AGENCY
FORT BLISS, TX 79916
ATTN MONA-WE

DIRECTOR
BMD ADVANCED TECH CTR
HUNTSVILLE, AL 35807
ATTN ATC-T, M CAPPS

DIRECTOR
BMD ADVANCED TECH CTR
HUNTSVILLE, AL 35807
ATTN ATC-O, W. DAVIES

DEP.CHIEF OF STAFF FOR RSCH, DEV&ACQ
DEPARTMENT OF THE ARMY
WASHINGTON DC 20310
ATTN MCB DIVISION

DEP.CHIEF OF STAFF FOR TSCH, DEV&ACQ
DEPARTMENT OF THE ARMY
WASHINGTON, DC 20310
ATTN DAMA-CSZ-C

DEP.CHIEF OF STAFF FOR RSCH, DEV&ACQ
DEPARTMENT OF THE ARMY
WASHINGTON DC 20310
ATTN DAMA-WSZC

DIRECTOR
U S ARMY BALLISTIC RESEARCH LABS
ABERDEEN PROVING GROUNDS,MD 21005
ATTN DRXRD-AM, G. KELLER

DIRECTOR
U S ARMY BALLISTIC RESEARCH LABS
ABERDEEN PROVING GROUNDS,MD 21005
ATTN DRXRD-BSP, J. HEIMERL

DIRECTOR
U S ARMY BALLISTIC RESEARCH LABS
ABERDEEN PROVING GROUNDS, MD 21005
ATTN JOHN MESTER

DIRECTOR
U S ARMY BALLISTIC RESEARCH LABS
ABERDEEN PROVING GROUNDS, MD 21005
ATTN TECH LIBRARY

COMMANDER
U S ARMY ELECTRONICS COMMAND
FOR MONMOUTH, N.J. 37703
ATTN INST FOR EXPL RESEARCH

COMMANDER
U S ARMY ELECTRONICS COMMAND
FOR MONMOUTH, N.J. 37703
ATTN DRSEL

COMMANDER
U S ARMY ELECTRONICS COMMAND
FOR MONMOUTH, N.J. 37703
ATTN STANLEY KRONENBERGER

COMMANDER
U S ARMY ELECTRONICS COMMAND
FORT MONMOUTH, N.J. 37703
ATTN WEAPONS EFFECTS SECTION

COMMANDER
US ARMY FOREIGN SCIENCE & TECH CTR
220 7TH STREET, NE
CHARLOTTESVILLEVA 29901
ATTN ROBERT JONES

CHIEF
US ARMY RESEARCH OFFICE
P.O. BOX 12211
TRIANGLE PARK, N.C. 27709
ATTN ROBERT MACE

COMMANDER
NAVAL OCEANS SYSTEMS CENTER
SAN DIEGO, CA 92152
ATTN CODE 2200 ILAN ROTHMULLER

COMMANDER
NAVAL OCEANS SYSTEMS CENTER
SAN DIEGO, CA 92152
ATTN CODE 2200 WILLIAM MOLER

COMMANDER
NAVAL OCEANS SYSTEMS CENTER
SAN DIEGO, CA 92152
ATTN CODE 2200 HERBERT HUGHES

COMMANDER
NAVAL OCEANS SYSTEMS CENTER
SAN DIEGO, CA 92152
ATTN CODE 2200 RICHARD PAPPERT

COMMANDER
NAVAL OCEANS SYSTEMS CENTER
SAN DIEGO, CA 92152
ATTN CODE 2200 JURGEN R RICHTER

DIRECTOR
NAVAL RESEARCH LABORATORY
WASHINGTON, DC 20375
ATTN CODE 7712 DOUGLAS P MCNUTT

DIRECTOR
NAVAL RESEARCH LABORATORY
WASHINGTON, DC 20375
ATTN CODE 7701 JACK D BROWN

DIRECTOR
NAVAL RESEARCH LABORATORY
WASHINGTON, DC 20375
ATTN CODE 2600 TECH LIB

DIRECTOR
NAVAL RESEARCH LABORATORY
WASHINGTON, DC 20375
ATTN CODE 7127 CHARLES Y JOHNSON

DIRECTOR
NAVAL RESEARCH LABORATORY
WASHINGTON, DC 20375
ATTN CODE 7700 TIMOTHY P COFFEY

DIRECTOR
NAVAL RESEARCH LABORATORY
WASHINGTON, DC 20375
ATTN CODE 7709 WAHAB ALI

DIRECTOR
NAVAL RESEARCH LABORATORY
WASHINGTON DC 20375
ATTN CODE 7750 DARRELL F STROBEL

DIRECTOR
NAVAL RESEARCH LABORATORY
WASHINGTON, DC 20375
ATTN CODE 7750 PAUL JULUENNE

DIRECTOR
NAVAL RESEARCH LABORATORY
WASHINGTON, DC 20375
ATTN CODE 7750 J. FEDDER

DIRECTOR
NAVAL RESEARCH LABORATORY
WASHINGTON, DC 20375
ATTN CODE 7750 S. OSSAKOW

DIRECTOR
NAVAL RESEARCH LABORATORY
WASHINGTON, DC 20375
ATTN CODE 7750 J. DAVIS

COMMANDER
NAVAL SURFACE WEAPONS CENTER
WHITE OAK, SILVER SPRING, MD 20910
ATTN CODE WA501 NAVY NUC PRGMS OFF

COMMANDER
NAVAL SURFACE WEAPONS CENTER
WHITE OAK, SILVER SPRING, MD 20910
ATTN TECHNICAL LIBRARY

SUPER INTENDENT
NAVAL POST GRADUATE SCHOOL
MONTEREY, CA 93940
ATTN TECH REPORTS LIBRARIAN

COMMANDER
NAVAL ELECTRONICS SYSTEMS COMMAND
NAVAL ELECTRONICS SYS COM HQS
ATTN PME 117

COMMANDER
NAVAL INTELLIGENCE SUPPORT CTR
4301 SUITLAND RD. BLDG 5
WASHINGTON, DC 20390
ATTN DOCUMENT CONTROL

AF GEOPHYSICS LABORATORY, AFSC
HANSCOM AFB, MA 01731
ATTN LKB KENNETH S W CHAMPION

AF GEOPHYSICS LABORATORY, AFSC
HANSCOM AFB, MA 01731
ATTN OPR ALVA T STAIR

AF GEOPHYSICS LABORATORY, AFSC
MANSCOM AFB MA 01731
ATTN OPR-1 J. ULWICK

AF GEOPHYSICS LABORATORY AFSC
HANSCOM AFB, MA 01731
ATTN OPR-1 R. MURPHY

AF GEOPHYSICS LABORATORY, AFSC
HANSCOM AFB, MA 01731
ATTN OPR-1 J. KENNEALY

AF GEOPHYSICS LABORATORY, AFSC
HANSCOM AFB, MA 01731
ATTN PHG JC MCCLAY

AF GEOPHYSICS LABORATORY, AFSC
HANSCOM AFB, MA 01731
ATTN LKD ROCCO NARCISI

AF GEOPHYSICS LABORATORY, AFSC
HANSCOM AFB, MA 01731
ATTN LKO, R. HUFFMAN

AF WEAPONS LABORATORY, AFSC
KIRTLAND, AFB, NM 87117
ATTN MAJ. GARY GANONG, DYM

COMMANDER
ASD
WPAFB, OH 45433
ATTN ASD-YH-EX LTC ROBERT LEVERETTE

SAMSO/AW
POST OFFICE BOX 92960
WORLDWAY POSTAL CENTER
LOS ANGELES, CA 90009
ATTN SZJ MAJOR LAWRENCE DOAN

SAMSO/SW
P.O. BOX 92960
WORLDWAY POSTAL CENTER
LOS, ANGELES, CA 90009
ATTN AW

AFTAC
PATRICK AFB, FL 32925
ATTN TECH LIBRARY

AFTAC
PATRICK AFB, FL 32925
ATTN TD

HQ
AIR FORCE SYSTEMS COMMAND
ANDREWS AFB
WASHINGTON, DC 20331
ATTN DLS

HQ
AIR FORCE SYSTEMS COMMAND
ANDREWS AFB
WASHINGTON, DC 20331
ATTN TECH LIBRARY

HQ
AIR FORCE SYSTEMS COMMAND
ANDREWS AFB
WASHINGTON, DC 20331
ATTN DLCAE

HQ
AIR FORCE SYSTEMS COMMAND
ANDREWS AFB
WASHINGTON, DC 20331
ATTN DLTW

HQ
AIR FORCE SYSTEMS COMMAND
ANDREWS AFB
WASHINGTON, DC 20331
ATTN DLXP

HQ
AIR FORCE SYSTEMS COMMAND
ANDREWS AFB
WASHINGTON, DC 20331
ATTN SDR

HQ USAF/RD
WASHINGTON, DC 20330
ATTN RDQ

COMMANDER
ROME AIR DEVELOPMENT CTR
GRIFFISS AFB, NY 13440
ATTN JJ. SIMONS OC SC

DIVISION OF MILITARY APPLICATION
U S ENERGY RSCH & DEV ADMIN
WASHINGTON, DC 20545
ATTN DOC CON

LOS ALAMOS SCIENTIFIC LABORATORY
P.O. BOX 1663
LOS, ALAMOS, NM 87545
ATTN DOC CON FOR R A JEFFRIES

LOS ALAMOS SCIENTIFIC LABORATORY
P.O. BOX 1663
LOS, ALAMOS, NM 87545
ATTN DOC CON FOR CR MEHL ORG 5230

LOS ALAMOS SCIENTIFIC LABORATORY
P.O. BOX 1663
LOS, ALAMOS, NM 87545
ATTN DOC CON FOR H V ARGO

LOS ALAMOS SCIENTIFIC LABORATORY
P.O. BOX 1663
LOS, ALAMOS, NM 87545
ATTN DOC CON FOR M. TIERNEY J-10

LOS ALAMOS SCIENTIFIC LABORATORY
P.O. BOX 1663
LOS, ALAMOS, NM 87545
ATTN DOC CON FOR ROBERT BROWNLEE

LOS ALAMOS SCIENTIFIC LABORATORY
P.O. BOX 1663
LOS, ALAMOS, NM 87545
ATTN DOC CON FOR WILLIAM MAIER

LOS ALAMOS SCIENTIFIC LABORATORY
P.O. BOX 1663
LOS ALAMOS, NM 87545
ATTN DOC CON FOR JOHN ZINN

LOS ALAMOS SCIENFIFIC LABORATORY
P.O. BOX 1663
LOS, ALAMOS, NM 87545
ATTN DOC CON FOR REFERENCE LIBRARY
ANN BEYER

SANDIA LABORATORIES
LIVERMORE LABORATORY
P.O. BOX 965
LIVERMORE, CA 94556
ATTN DOC CONTROL FOR
THOMAS COOK ORG 8000

SANDIA LABORATORIES
P.O. BOX 5800
ALBUQUERQUE, NM 87115
ATT DOC CONT. FOR
W.D. BROWN ORG 1353

SANDIA LABORATORIES
P.O. BOX 5800
ALBUQUERQUE, NM 87115
ATTN DOC CONT. FOR
L. ANDERSON ARG 1247

SANDIA LABORATORIES
P.O. BOX 5800
ALBUQUERQUE, NM 87115
ATTN DOC CONT.
FOR MORGAN KRAMMA ORG 5720

SANDIA LABORATORIES
P.O. BOX 5800
ALBUQUERQUE, NM 87115
ATTN DOC CONT.
FOR FRANK HUDSON ORG 1722

SANDIA LABORATORIES
P.O. BOX 5800
ALBUQUERQUE, NM 87115
ATTN DOC CONT.
FOR ORG 3422-1 SANDIA REPTS COLL.

ARGONNE NATIONAL LABORATORY
RECORDS CONTROL
9700 SOUTH CASS AVENUE
ARGONNE, IL 60439
ATTN DOC CON FOR A C WAHL

ARGONNE NATIONAL LABORATORY
RECORDS CONTROL
9700 SOUTH CASS AVENUE
ARGONNE, IL 60439
ATTN DOC CON FOR DAVID W GREEN

ARGONNE NATIONAL LABORATORY
RECORDS CONTROL
9700 SOUTH CASS AVENUE
ARGONNE, IL 60439
ATTN DOC CON FOR LIR SVCS RPTS SEC

ARGONNE NATIONAL LABORATORY
RECORDS CONTROL
9700 SOUTH CASS AVENUE
ARGONNE, IL 60439
ATTN DOC CON FOR S GARELNICK

ARGONNE NATIONAL LABORATORY
RECORDS CONTROL
9700 SOUTH CASS AVENUE
ARGONNE, IL 60439
ATTN DOC CON FOR GERALD T REEDY

UNIVERSITY OF CALIFORNIA
LAWRENCE LIVERMORE LABORATORY
P.O. BOX 808
LIVERMORE CA 94550
ATTN W.H. DUEWER GEN L-404

UNIVERSITY OF CALIFORNIA
LAWRENCE LIVERMORE LABORATORY
P.O. BOX 808
LIVERMORE CA 94550
ATTN JULIUS CHANG L-71

UNIVERSITY OF CALIFORNIA
LAWRENCE LIVERMORE LABORATORY
P.O. VOX 808
LIVERMORE CA 94550
G.R. HAUGEN L-404

UNIVERSITY OF CALIFORNIA
LAWRENCE LIVERMORE LABORATORY
P.O. BOX 808
LIVERMORE CA 94550
ATTN D.J. WUERBLES L-142

CALIFORNIA, STATE OF
AIR RESOURCE BOARD
9528 TELSTA AVE
AL MONTE, CA 91731
ATTN LEO ZAFONTE

CALIFORNIA INSTITUTE OF TECHNOLOGY
JET PROPULSION LABORATORY
4800 OAK GROVE DRIVE
PASADENA CA 91103
ATTN JOSEPH A JELLO

US ENERGY RSCH & DEV ADMIN
DIVISION OF HEADQUARTERS SERVICES
LIBRARY BRANCH G-043
WASHINGTON, DC 20545
ATTN DOC CON FOR CLASS TECH LIB

DEPARTMENT OF TRANSPORTATION
OFFICE OF THE SECRETARY
TAD-44,1, ROOM 10402-R
400 7TH STREET S.W.
WASHINGTON, DC 20590
ATTN SAMUEL C CORONITI

NASA
GODDARD SPACE FLIGHT CENTER
GREENBELT, MD 20771
ATTN A C AIKEN

NASA
GODDARD SPACE FLIGHT CENTER
GREENBELT, MD 20771
ATTN A TEMPKIN

NASA
GODDARD SPACE FLIGHT CENTER
GREENBELT, MD 20771
ATTN A J BAUER

NASA
GODDARD SPACE FLIGHT CENTER
GREENBELT, MD 20771
ATTN TECHNICAL LIBRARY

NASA
GADDARD SPACE FLIGHT CENTER
GREENBELT, MD 20771
ATTN J. SIRY

NASA
600 INDEPENDENCE AVENUE S W
WASHINGTON, DC 20546
ATTN A GESSOW

NASA
600 INDEPENDENCE AVENUE S W
WASHINGTON, DC 20546
ATTN D P CAUFFMAN

NASA
600 INDEPENDENCE AVENUE S W
WASHINGTON, DC 20546
ATTN LTC D R HALLENBECK CODE SG

NASA
600 INDEPENDENCE AVENUE S W
WASHINGTON, DC 20546
ATTN R FELLOWS

NASA
600 INDEPENDENCE AVENUE S W
WASHINGTON, DC 20546
ATTN A SCHARDT

NASA
600 INDEPENDENCE AVENUE S W
WASHINGTON, DC 20546
ATTN M TEPPER

NASA
LANGLEY RESEARCH CENTER
LANGLEY STATION
HAMPTON, VA 23365
ATTN CHARLES SCHEXNAYDER MS-168

NASA
AMES RESCH CENTER
MOFFETT FIELD, CA 90435
ATTN N-254-4 WALTER L. STARR

NASA
AMES RESEARCH CENTER
MOFFETT FIELD, CA 94035
ATTN N-254-4 R WHITTEN

NASA
AMES RESEARCH CENTER
MOFFETT FIELD, CA 94035
ATTN N-254-4 ILIA G POPPOFF

NASA
AMES RESEARCH CENTER
MOFFETT FIELD, CA 94036
ATTN N-254-3 NEIL H FARLOW

NASA
GEORGE C MARSHALL
SPACE FLIGHT CENTER
HUNTSVILLE, AL 35812
ATTN C R BALCHER

NASA
GEORGE C MARSHALL
SPACE FLIGHT CENTER
HUNTSVILLE, AL 35812
ATTN H STONE

NASA
GEORGE C MARSHALL
SPACE FLIGHT CENTER
HUNTSVILLE, AL 35812
ATTN W A ORAN

NASA
GEORGE C MARSHALL
SPACE FLIGHT CENTER
HUNTSVILLE, AL 35812
ATTN CODE ES22 JOHN WATTS

NASA
GEORGE C MARSHALL
SPACE FLIGHT CENTER
HUNTSVILLE, AL 35812
ATTN W T ROBERTS

NASA
GEORGE C MARSHALL
SPACE FLIGHT CENTER
HUNTSVILLE, AL 35812
ATTN R D HUDSON

NASA
GEORGE C MARSHALL
SPACE FLIGHT CENTER
HUNTSVILLE, AL 35812
ATTN R CHAPPELL

ALBANY METALLURGY RESCH CENTER
U S BUREAU OF MINES
P.O. BOX 70
ALBANY, OR 97321
ATTN ELEANOR ARSHIRE

CENTRAL INTELLIGENCE AGENCY
ATTN RD/SI RM 5G48 HQ BLDG
WASHINGTON DC 20505
ATTN NED/OSI-2G4R HQS

DEPARTMENT OF COMMERCE
NATIONAL BUREAU OF STANDARDS
WASHINGTON, DC 20234
ATTN SEC OFFICER FOR
ATTN JAMES DEVOE

DEPARTMENT OF COMMERCE
NATIONAL BUREAU OF STANDARDS
WASHINGTON, DC 20234
ATTN SEC OFFICER
STANLEY ARRAMOWITZ

DEPARTMENT OF COMMERCE
NATIONAL BUREAU OF STANDARDS
WASHINGTON, DC 20234
ATTN SEC OFFICER FOR
ATTN J COOPER

DEPARTMENT OF COMMERCE
NATIONAL BUREAU OF STANDARDS
WASHINGTON, DC 20234
ATTN SEC OFFICER FOR
ATTN GEORGE A SINNATT

DEPARTMENT OF COMMERCE
NATIONAL BUREAU OF STANDARDS
WASHINGTON, DC 20234
ATTN SEC OFFICER FOR
ATTN K KESSLER

DEPARTMENT OF COMMERCE
NATIONAL BUREAU OF STANDARDS
WASHINGTON, DC 20234
ATTN SEC OFFICER FOR
ATTN M KRAUSS

DEPARTMENT OF COMMERCE
NATIONAL BUREAU OF STANDARDS
WASHINGTON, DC 20234
ATTN SEC OFFICER FOR
ATTN LEWIS H GEVANTMAN

DEPARTMENT OF COMMERCE
NATIONAL BUREAU OF STANDARDS
WASHINGTON, DC 20234
ATTN SEC OFFICER FOR
ATTN JAMES DEVOE

NATIONAL OCEANIC & ATMOSPHERIC ADMIN
ENVIRONMENTAL RESEARCH LABORATORIES
DEPARTMENT OF COMMERCE
BOULDER, CO 80302
ATTN GEORGE C REID AERONOMY LAB

NAT OCEANIC & ATMOSPHERIC ADMIN
ENVIRONMENTAL RESEARCH LABORATORIES
DEPARTMENT FO COMMERCE
BOULDER, CO 80302
ATTN ELDON FERGUSON

NAT OCEANIC & ATMOSPHERIC ADMIN
ENVIRONMENTAL RESEARCH LABORATORIES
DEPARTMENT FO COMMERCE
BOULDER, CO 80302
ATTN FRED FEHSENFELD

AERO-CHEM RESCH LABS, INC
P.O. BOX 12
PRINCETON, NJ 08540
ATTN A FONTIJN

AERO-CHEM RESCH LABS, INC
P.O. BOX 12
PARINCETON, NJ 08540
ATTN H PERGAMENT

AERODYNE RESEARCH, INC
BEDFORD RESEARCH PARK
CROSBY DRIVE
BEDFORD, MA 01731 ATTN F BIEN

AERODYNE RESEARCH, INC
BEDFORD RESEARCH PARK
CROSBY DRIVE
BEDFORD, MA 01731 ATTN M CAMAC

AERONOMY CORPORATION
217 S NEIL STREET
CHAMPAIGN, IL 61820
ATTN A BOWHILL

AEROSPACE CORPORATION
P.O. BOX 92957
LOS ANGELES, CA 90009
ATTN N COHEN

AEROSPACE CORPARATION
P.O. BOX 92957
LOS ANGELES, CA 90009
ATTN HARRIS MAYER

AEROSPACE CORPORATION
P.O. BOX 92957
LOS ANGELES, CA 90009
ATTN SIDNEY W KASH

AEROSPACE CORPORATION
P.O. BOX 92957
LOS ANGELES, CA 90009
ATTN T WIDHOPH

AEROSPACE CORPORATION
P.O. BOX 92957
LOS ANGELES, CA 90009
ATTN R J MCNEAL

AEROSPACE CORPORATION
P.O. BOX 92957
LOS ANGELES, CA 90009
ATTN R GROVE

AEROSPACE CORPORATION
P.O. BOX 92957
LOS ANGELES, CA 90009
ATTN IRVING M GARFUNKEL

AEROSPACE CORPORATION
P.O. BOX 92957
LOS ANGELES, CA 90009
ATTN THOMAS D TAYLOR

AEROSPACE CORPORATION
P.O. BOX 92957
LOS ANGELES, CA 90009
ATTN V JOSEPHSON

AEROSPACE CORPORATION
P.O. BOX 92957
LOS ANGELES, CA 90009
ATTN JULIAN REINMEIMER

AEROSPACE CORPORATION
P.O. BOX 92957
LOS ANGELES, CA 90009
ATTN R D RAWCLIFFE

AVCO-EVERETT RESCH LAB INC
2385 REVERE BEACH PARKWAY
EVERETT, MA 02149
ATTN TECHNICAL LIBRARY

AVCO-EVERETT RESCH LAB INC
2385 REVERE BEACH PARKWAY
EVERETT, MA 02149
ATTN GEORGE SUTTON

AVCO-EVERETT RESCH LAB INC
2385 REVERE BEACH PARKWAY
EVERETT, MA 02149
ATTN C W VON ROSENBERG JR

BATTELLE MEMORIAL INSTITUTE
505 KING AVENUE
COLUMBUS, OH 43201
ATTN DONALD J HAMMAN

BATTELLE MEMORIAL INSTITUTE
505 KING AVENUE
COLUMBUS, OH 43201
ATTN DONALD J HAM

BATTELLE MEMORIAL INSTITUTE
505 KING AVENUE
COLUMBUS, OH 43201
ATTN STOIAC

BATTELLE MEMORIAL INSTITUTE
505 KING AVENUE
COLUMBUS, OH 43201
ATTN RICHARD K THATCHER

BROWN ENGINEERING COMPANY INC
CUMMINGS RESCH PARK
HUNTSVILLE, AL 35807
ATTN N PASSINO

THE TRUSTEES OF BOSTON COLLEGE
CHESTNUT HILL CAMPUS
CHESTNUT HILL, MA 02167
ATTN CHAIRMAN DEPT OF CHEM

BROWN ENGINEERING COMPANY INC
COMMINGS RESEARCH PARK
HUNTSVILLE, AL 35807
ATTN RONALD PATRICK

CALIFORNIA AT RIVERSIDE, UNIV OF
RIVERSIDE, CA 92502
ATTN ALAN C LLOYD

CALIFORNIA AT RIVERSIDE, UNIV OF
RIVERSIDE, CA 92502
ATTN JAMES N PITTS JR

CALIFORNIA AT SAN DIEGO, UNIV OF
3175 MIRAMAR ROAD
LA JOLLA, CA 92037
ATTN S C LIN

CALIFORNIA UNIVERSITY OF
BERKELEY CAMPUS ROOM 318
SPROUL HALL
BERKELEY, CA 94720
ATTN SEC OFFICER FOR HAROLD JOHNSTON

CALIFORNIA UNIVERSITY OF
BERKELEY CAMPUS ROOM 318
SPROUL HALL
BERKELEY, CA 94720
ATTN SEC OFFICER FOR F MOZER

CALIFORNIA UNIVERSITY OF
BERKELEY CAMPUS ROOM 318
SPROUL HALL
BERKELEY, CA 94720
ATTN SEC OFFICER FOR DEPT OF CHAM
W H MILLER

CALIFORNIA, STATE OF
AIR RESOURCES BOARD
9528 TELSTAR AVENUE
EL MONTE, CA 91731
ATTN LEO ZAFONTE

CALSPAN CORPORATION
P.O. BOX 235
BUFFALO, NY 14224
ATTN C E TREANOR

CALSPAN CORPORATION
P.O. BOX 235
BUFFALO, NY 14221
ATTN G C VALLEY

CALSPAN CORPORATION
P.O. BOX 235
BUFFALO, NY 14221
ATTN M G DUNN

CALSPAN CORPORATION
P.O. BOX 235
BUFFALO, NY 14221
ATTN W WURSTER

COLORADO, UNIVERSITY OF
OFFICE OF CONTRACTS AND GRANTS
380 ADMINISTRATIVE ANNEX
BOULDER, CO 80302
ATTN A PHELPS JILA

COLORADO, UNIVERSITY OF
OFFICE OF CONTRANCTS AND GRANTS
380 ADMINISTRATIVE ANNEX
BOULDER, CO 80302
ATTN JEFFREY B PEARCE LASP

COLORADO, UNIVERSITY OF
OFFICE OF CONTRANCT AND GRANTS
380 ADMINISTRATIVE ANNEX
BOULDER, CO 80302
ATTN C BEATY JILA

COLORADO, UNIVERSITY OF
OFFICE OF CONTRACTS AND GRANTS
380 ADMINISTRATIVE ANNEX
BOULDER, CO 80302
ATTN C LINEBERGER JILA

COLORADO, UNIVERSITY OF
OFFICE OF CONTRACTS AND GRANTS
380 ADMINISTRATIVE ANNEX
BOULDER, CO 80302
ATTN CHARLES A BARTH LASP

COLUMBIA UNIVERSITY, THE TRUSTEES
IN THE CITY OF NEW YORK
LA MONT DOHERTY GEOLOGICAL
OBSERVATORY-TORREY CLIFF
PALISADES, NY 19064
ATTN B PHELAN

COLUMBIA UNIVERSITY, THE TRUSTEES
OF THE CITY OF NEW YORK
116TH STREET & BROADWAY
NEW YORK, NY 10027
ATTN RICHARD N ZARE

COLUMBIA UNIV, THE TRUSTEES OF
CITY OF NEW YORK
116TH & BROADWAY
NEW YORK, NY 10027
ATTN SEC OFFICER H M FOLEY

CONCORD SCIENCES
P.O. BOX 119
CONCORD, MA 01742
ATTN EMMETT A SUTTON

DENVER, UNIVERSITY OF
COLORADO SEMINARY
DENVER RESEARCH INSTITUTE
P.O. BOX 10127 DENVER, CO 80210
ATTN SEC OFFICER FOR MR VAN ZYL

DENVER, UNIVERSITY OF
COLORADO SEMINARY
DENVER RESEARCH INSTITUTE
P.O. BOX 10127 DENVER, CO 80210
ATTN SEC OFFICER FOR DAVID MURCRAY

GENERAL ELECTRIC COMPANY
TEMPO-CENTER FOR ADVANCED STUDIES
816 STATE STREET (P.O. DRAWER QQ)
SANTA BARBARA, CA 93102
ATTN DASAIC

GENERAL ELECTRIC COMPANY
TEMPO-CENTER FOR ADVANCED STUDIES
816 STATE STREET (P.O. DRAWER QQ)
SANTA BARBARA, CA 93102
ATTN WARREN S KNAPP

GENERAL ELECTRIC COMPANY
TEMPO-CENTER FOR ADVANCED STUDIES
816 STATE STREET (P.O. DRAWER)
SANTA BARBARA, CA 93102
ATTN TIM STEPHENS

GENERAL ELECTRIC COMPANY
TEMPO-CENTER FOR ADVANCED STUDIES
816 STATE STREET (P.O. DRAWER QQ)
SANTA BARBARA, CA 93102
ATTN DON CHANDLER

GENERAL ELECTRIC COMPANY
TEMPO-CENTER FOR ADVANCED STUDIES
816 STATE STREET (P.O. DRAWER QQ)
SANTA BARBARA, CA 93102
ATTN B CAMBILL

GENERAL ELEC. CO.
SPACE DIVISION
VALLEY FORGE SPACE CTR
GODDARD BLVD
KING OF PRUSSIA
P.O. BOX 8555
PHILADELPHIA, PA 19101
ATTN M H BORTNER, SPACE SCIENCE LAB

GENERAL ELEC. CO.
SPACE DIVISION
VALLEY FORGE SPACE CENTER
GODDARD BLVD. KING OF PRUSSIA
P.O. BOX 8555
PHILADELPHIA, PA 19101
ATTN J BURNS

GENERAL ELEC. CO.
SPACE DIVISION
VALLEY FORGE SPACE CENTER
GODDARD BLVD KING OF PRUSSIA
P.O. BOX 8555
PHILADELPHIA, PA 19101
ATTN F ALYEA

GENERAL ELEC. CO.
SPACE DIVISION
VALLEY FORGE SPACE CENTER
GODDARD BLVD KING OF PRUSSIA
P.O. BOX 8555
PHILADELPHIA, PA 19101
ATTN P ZAVITSANDS

GENERLA ELEC. CO.
SPACE DIVISION
VALLEY FORGE SPACE CENTER
GODDARD BLVD KING OF PRUSSIA
P.O. BOX 8555
PHILADELPHIA, PA 19101
ATTN R H EDSALL

GENERAL ELEC. CO.
SPACE DIVISION
VALLEY FORGE SPACE CENTER
GODDARD BLVD KING OF PRUSSIA
P.O. BOX 8555
PHILADELPHIA, PA 19101
ATTN T BAURER

GENERAL RESEARCH CORPORATION
P.O. BOX 3587
SANTA BARBARA, CA 93105
ATTN JOHN ISE JR

GEOPHYSICAL INSTITUTE
UNIVERSITY OF ALASKA
FAIRBANKS, AK 99701
ATTN D HENDERSON

GEOPHYSICAL INSTITUTE
UNIVERSITY OF ALASKA
FAIRBANKS, AK 99701
ATTN J S WAGNER PHYSICS DEPT

GEOPHYSICAL INSTITUTE
UNIVERSITY OF ALASKA
FAIRBANKS, AK 99701
ATTN B J WATKINS

GEOPHYSICAL INSTITUTE
UNIVERSITY OF ALASKA
FAIRBANKS, AK 99701
ATTN T N DAVIS

GEOPHYSICAL INSTITUTE
UNIVERSITY OF ALASKA
FAIRBANKS, AK 99701
ATTN R PARTHASARATHY

GEOPHYSICAL INSTITUTE
UNIVERSITY OF ALASKA
FAIRBANKS, AK 99701
ATTN NEAL BROWN

LOWELL, UNIVERSITY OF
CENTER FOR ATMOSPHERIC RESEARCH
450 AIKEN STREET
LOWELL, MA 01854
ATTN G T BEST

LOCKHEED MISSILES & SPACE COMPANY
3251 HANOVER STREET
PALA ALTO, CA 94394
ATTN JOHN KUMER DEPT 52-54

LOCKHEED MISSILES & SPACE COMPANY
3251 HANOVER STREET
PALO, ALTO, CA 94304
ATTN KIMER DEPT 52-54

LOCKHEED MISSILES & SPACE COMPANY
3251 HANOVER STREET
PALO, ALTO, CA 94304
ATTN JOHN B CLADIS DEPT 52-12

LOCK HEED MISSILES & SPACE CO
3251 HANOVER STREET
PALO, ALTO, CA 94304
ATTN GILLY M MCCORMAC DEPT 52-54

LOCKHEED MISSILES & SPACE CO
3251 HANOVER STREET
PALO, ALTO, CA 94304
ATTN TOM JAMES DEPT 52-54

LOCKHEED MISSILES & SPACE CO
3251 HANOVER STREET
PALO, ALTO, CA 94304
ATTN J B REAGAN D/52-12

LOCKHEED MISSILES & SPACE CO
3251 HANOVER STREET
PALO, ALTO, CA 94304
ATTN MARTIN WALT DEPT 52-10

LOCKHEED MISSILES & SPACE CO
3251 HANOVER STREET
PALO, ALTO, CA 94304
ATTN RICHARD G JOHNSON DEPT 52-12

LOCKHEED MISSILES & SPACE CO
3251 HANOVER STREET
PALO, ALTO, CA 94304
ATTN ROBERT D SEARS DEPT 52-14

LOCKHEED MISSILES & SPACE CO
3251 HANOVER STREET
PALO, ALTO, CA 94304
ATTN J R WINKLER

INSTITUTE FOR DEFENSE ANALYSE
400 ARMY-NAVY DRIVE
ARLINGTON, VA 22202
ATTN ERNEST BAUER

INSTITUTE FOR DEFENSE ANALYSE
400 ARMY-NAVY DRIVE
ARLINGTON, VA 22202
ATTN HANS WOLFHARD

MISSION RESEARCH CORPORATION
735 STATE STREET
SANTA BARBARA, CA 93101
ATTN D ARCHER

MISSION RESEARCH CORPORATION
735 STATE STREET
SANTA BARBARA, CA 93101
ATTN D FISCHER

MISSION RESEARCH CORPORATION
735 STATE STREET
SANTA BARBARA, CA 93101
ATTN M SCHEIBE

MISSION RESEARCH CORPORATION
735 STATE STREET
SANTA BARBARA, CA 93101
ATTN D SAPPENFIELD

MISSION RESEARCH CORPORATION
735 STATE STREET
SANTA BARBARA, CA 93101
ATTN D SOWLE

PHOTOMETRIC, INC.
442 MARETT ROAD
LEXINGTON, MA 02173
ATTN IRVING L KOFSKY

PHYSICAL DYNAMICS INC.
P.O. BOX 1069
BERKELEY, CA 94701
ATTN J B WORKMAN

PHYSICAL DYNAMICS INC.
P.O. BOX 1069
BERKELEY, CA 94701
ATTN A THOMPSON

PHYSICAL SCIENCES, INC.
30 COMMERCE WAY
WOBURN, MA 01801
ATTN KURT WRAY

PHYSICAL SCIENCES, INC.
30 COMMERCE WAY
WOBURN, MA 01801
ATTN R L TAYLOR

PHYSICAL SCIENCES, INC.
30 COMMERCE WAY
WOBURN, MA 01801
ATTN G CALEDONIA

PHYSICS INTERNATIONAL COMPANY
2700 MERCED STREET
SAN LEANDRO, CA 94577
ATTN DOC CON FOR TECH LIB

PITTSBURGH, UNIV OF
OF THE COMWLTH SYS OF HIGHER EDUC
CATHEDRAL OF LEARNING
PITTSBURGH, PA 15213
ATTN WADE L FITE

PITTSBURGH, UNIVERSITY OF
OF THE COMWLTH SYS OF HIGHER EDUC
CATHEDRAL OF LEARNING
PITTSBURGH, PA 15213
ATTN MANFRED A BIONDI

PITTSBURGH, UNIVERSITY OF
OF THE COMWLTH SYS OF HIGHER EDUC
CATHEDRAL OF LEARNING
PITTSBURGH, PA 15213
ATTN FREDERICK KAUFMAN

PITTSBURGH, UNIVERSITY OF
OF THE COMWLTH SYS OF HIGHER EDUC
CATHEDRAL OF LEARNING
PITTSBURGH, PA 15213
ATTN EDWARD GERJUOY

PRINCETON UNIV, THE TRUSTEES OF
FORRESTAL CAMPUS LIBRARY
BOX 710
PRINCETON UNIVERSITY
PRINCETON, NJ 08540
ATTN ARNOLD J KELLY

R & D ASSOCIATES
P.O. BOX 9695
MARINA DEL REY, CA 90291
ATTN RICHARD LATTER

R & D ASSOCIATES
P.O. BOX 9695
MARINA DEL REY, CA 90291
ATTN R G LINDGREN

R & D ASSOCIATES
P.O. BOX 9695
MARINA DEL REY, CA 90291
ATTN BRYAN GABBARD

R & D ASSOCIATES
P.O. BOX 9695
MARINA DEL REY, CA 90291
ATTN H A DRY

R & D ASSOCIATES
P.O. BOX 9695
MARINA DEL REY, CA 90291
ATTN ROBERT E LELEVIER

R & D ASSOCIATES
P.O. BOX 9695
MARINA DEL REY, CA 90291
ATTN R P TURCO

R & D ASSOCIATES
P.O. BOX 9695
MARINA DEL REY, CA 90291
ATTN ALBERT L LATTER

R & D ASSOCIATES
P.O. BOX 9695
MARINA DEL REY, CA 90291
ATTN FORREST GILMORE

R & D ASSOCIATES
P.O. BOX 9695
MARINA DEL REY, CA 90291
ATTN D DEE

R & D ASSOCIATES
1815 N. FT. MYER DRIVE
11TH FLOOR
ARLINGTON, VA 22209
ATTN HERBERT J MITCHELL

R & D ASSOCIATES
1815 N. FT. MYER DRIVE
11TH FLOOR
ARLINGTON, VA 22209
ATTN J W ROSENGREN

RAND CORPORATION
1700 MAIN STREET
SANTA MONICA, CA 90406
ATTN CULLEN CRAIN

SCIENCE APPLICATIONS, INC.
P.O. BOX 2351
LA JOLLA, CA 92038
ATTN DANIEL A HAMLIN

SCIENCE APPLICATIONS, INC.
P.O. BOX 2351
LA JOLLA, CA 92038
ATTN DAVID SACHS

SPACE DATA CORPORATION
1331 SOUTH 26TH STREET
PHOENIX, AZ 85034
ATTN EDWARD F ALLEN

STANFORD RSCH INSTITUTE INTERNATIONAL
333 RAVENSWOOD AVENUE
MENLO PARK, CA 94025
ATTN M BARON

STANFORD RSCH INSTITUTE INTL
333 RAVENSWOOD AVENUE
MENLO PARK, CA 94025
ATTN L LEADABRAND

STANFORD RSCH INSTITUTE INTL
333 RAVENSWOOD AVENUE
MENLO PARK, CA 94025
ATTN WALTER H CHESTNUT

STANFORD RSCH INSTITUTE INTL
1611 NORTH KENT STREET
ARLINGTON, VA 22209
ATTN WARREN W BERNING

STANFORD RSCH INSTITUTE INTL
1611 NORTH KENT STREET
ARLINGTON, VA 22209
ATTN CHARLES HULBERT

TECHNOLOGY INTL CORPORATION
75 WIGGINS AVENUE
BEDFORD, MA 01730
ATTN W P BOQUIST

UNITED TECHNOLOGIES CORP
755 MAIN STREET
HARTFORD, CT 06103
ATTN H MICHELS

UNITED TECHNOLOGIES CORP
755 MAIN STREET
HARTFORD, CT 06103
ATTN ROBERT HBULLIS

UTAH STATE UNIVERSITY
LOGAN, UT 84321
ATTN DORAN BAKER

UTAH STATE UNIVERSITY
LOGAN, UT 84321
ATTN KAY BAKER

UTAH STATE UNIVERSITY
LOGAN, UT 84321
ATTN C WYATT

UTAH STATE UNIVERSITY
LOGAN, UT 84321
ATTN D BURT

VISIDYNE, INC.
19 THIRD AVENUE
NORTHWEST INDUSTRIAL PARK
BURLINGTON, MA 01803
ATTN HENRY J SMITH

VISIDYNE, INC.
19 THIRD AVENUE
NORTHWEST INDUSTRIAL PARK
BURLINGTON, MA 01803
ATTN J W CARPENTER

VISIDYNE, IND.
19 THIRD AVENUE
NORTHWEST INDUSTRIAL PARK
BURLINGTON, MA 01803
ATTN WILLIAM REIDY

VISIDYNE, INC.
19 THIRD AVENUE
NORTHWEST INDUSTRIAL PARK
BURLINGTON, MA 01803
ATTN T C DEGGES

VISIDYNE, INC.
19 THIRD AVENUE
NORTHWEST INDUSTRIAL PARK
BURLINGTON, MA 01803
ATTN CHARLES HUMPHREY

WAYNE STATE UNIVERSITY
1064 MACKENZIE HALL
DETROIT, MI 48202
ATTN PIETER K ROL
CHAM ENGR & MAT SCI

WAYNE STATE UNIVERSITY
1064 MACKENZIE HALL
DETROIT, MI 48202
ATTN R H KUMMLER

WAYNE STATE UNIVERSITY
DEPT. OF PHYSICS
DETROIT, MI 48202
ATTN WALTER E KAUPPILA

YALE UNIVERSITY
NEW HAVEN, CT 06520
ATTN ENGINEERING DEPARTMENT